Meteorol. Z. (Contrib. Atm. Sci.), Early Access DOI 10.1127/metz/2023/1154

Early Access Article

Linkages between Arctic and Mid-Latitude Weather and Climate: Unraveling the Impact of Changing Sea Ice and Sea Surface Temperatures during Winter

Ralf Jaiser[1*], M. Akperov[2], A. Timazhev[2], E. Romanowsky[1,3], D. Handorf[1] and I.I. Mokhov[2,4]

[1]Alfred Wegener Institute, Helmholtz Center for Polar and Marine Research, Potsdam, Germany
[2]A.M. Obukhov Institute of Atmospheric Physics, RAS, Moscow, Russia
[3]University of Potsdam, Institute of Physics and Astronomy, Potsdam, Germany
[4]Lomonosov Moscow State University, Moscow, Moscow, Russia.

(Manuscript received June 24, 2022; in revised form November 21, 2022; accepted November 23, 2022)

Abstract

The study addresses the question, if observed changes in terms of Arctic-midlatitude linkages during winter are driven by Arctic Sea ice decline alone or if the increase of global sea surface temperatures plays an additional role. We compare atmosphere-only model experiments with ECHAM6 to ERA-Interim Reanalysis data. The model sensitivity experiment is implemented as a set of four combinations of sea ice and sea surface temperature boundary conditions. Atmospheric circulation regimes are determined and evaluated in terms of their cyclone and blocking characteristics and changes in frequency during winter. As a prerequisite, ECHAM6 reproduces general features of circulation regimes very well. Tropospheric changes induced by the change of boundary conditions are revealed and further impacts on the large-scale circulation up into the stratosphere are investigated. In early winter, the observed increase of atmospheric blocking in the region between Scandinavia and the Urals are primarily related to the changes in sea surface temperatures. During late winter, we find a weakened polar stratospheric vortex in the reanalysis that further impacts the troposphere. In the model sensitivity study a climatologically weakened polar vortex occurs only if sea ice is reduced and sea surface temperatures are increased together. This response is delayed compared to the reanalysis. The tropospheric response during late winter is inconclusive in the model, which is potentially related to the weak and delayed response in the stratosphere. The model experiments do not reproduce the connection between early and late winter as interpreted from the reanalysis. Potentially explaining this mismatch, we identify a discrepancy of ECHAM6 to reproduce the weakening of the stratospheric polar vortex through blocking induced upward propagation of planetary waves.

Keywords: Weather regimes, Blocking, Cyclones, Wave Propagation, Stratosphere

1 Introduction

Impacts from linkages between the Arctic and mid-latitudes are a fundamental feature of a heterogeneously warming global climate, while at the same time they are embedded in the climate system that is dominated by natural variability. In this context, Overland et al. (2021) find that conclusions on the state of Arctic/midlatitude weather linkages are inconsistent. Changes in the temperature gradients between high and low latitudes are the fundamental driver of the global atmospheric circulation including cyclone/anticyclone activity in the mid and high latitudes (e.g., Akperov et al., 2019; Day et al., 2018; He et al., 2014). But neither Arctic Amplification itself nor its implications for global climate are fully understood, leading to huge endeavors to unravel the open questions with observational and modelling approaches (Cohen et al., 2020; Jung et al., 2016; Wendisch et al., 2017; MOSAiC). A major focal point of research is, whether Arctic Amplification has a significant influence on mid-latitude severe winter weather. While observational evidence largely confirms the hypothesis that Arctic Amplification contributes to mid-latitude winter continental cooling, only few modelling studies support this conclusion (Cohen et al., 2020). In a more general global warming perspective, early model results presented in (Lupo et al., 1997) show the manifestation of winter cooling anomalies in midlatitudes over continents as a common consequence of global warming. The mechanism involves a weakened zonal circulation with more long-lived and intense atmospheric blockings over the continents in winter as a consequence of the warmer troposphere (see also Mokhov and Petukhov, 1997; Mokhov and Semenov, 2016).

Our previous studies support the observational evidence by comparing the large-scale conditions prior to the year 2000 with relatively high sea ice concentration (SIC) in the Arctic to later years with relatively low SIC. Baroclinic processes translate changed conditions at the surface in terms of reduced SIC and higher surface air temperatures to larger scales (Jaiser et al., 2012).

*Corresponding author: Ralf Jaiser, Alfred Wegener Institute, Helmholtz Center for Polar and Marine Research, Telegrafenberg A45, 14473 Potsdam, Germany, e-mail: ralf.jaiser@awi.de

Gebrüder Borntraeger Science Publishers, Stuttgart, www.borntraeger-cramer.com

Here, the most prominent feature is a climatological shift to mean sea level pressure (MSLP) anomalies during winter that resemble a negative phase of Arctic Oscillation (AO) during the most recent decades. This implies weakened and more meandering jet streams and thus potential for more extreme weather over the continents as described by Francis and Vavrus (2012). Changed large-scale circulation patterns are also found in the stratosphere where a weakened stratospheric polar vortex is observed, as a result of enhanced upward wave fluxes from planetary waves (Jaiser et al., 2013). By evaluating model experiments from Nakamura et al. (2015) with the atmospheric general circulation model for Earth Simulator (AFES), we confirmed that sea ice anomalies have the potential to exert strong upward wave anomalies during early winter that disturb the polar vortex (Jaiser et al., 2016). The downward influence of the disturbed vortex than explains the observed negative phase of the AO during late winter through descending anomalies as described by Baldwin and Dunkerton (2001). Crasemann et al. (2017) implemented a regime analysis on the same model experiments with a focus on the North Atlantic and Eurasian sector. They confirm a late winter shift to a higher frequency of occurrence of circulation regimes that resemble the negative phase of the North Atlantic Oscillation (NAO) related to low SIC. During early winter they find an increase in frequency of circulation regimes that are related to atmospheric blocking in the Scandinavian region. Martius et al. (2009) found that blockings impact stratospheric variability dependent on their geographical location. In particular blocking highs in the Euro-Atlantic sector lead to upward planetary wave propagation impacting the stratosphere. This sequence of blockings and upward wave propagation in early winter, a weakened polar vortex during mid-winter and a following impact on the troposphere with negative AO-like anomalies during late winter is known as the stratospheric pathway for linkages between Arctic and mid-latitudes.

A complementing study with ECHAM6 found only a weak response in terms of a shift to a negative phase of the AO related to SIC and snow cover changes (Handorf et al., 2015). This has been attributed to a weak resemblance of characteristics of planetary wave propagation. A multi-model studies by Screen et al. (2018) further concludes with the open question if the response by climate models to Arctic sea-ice loss is too weak. Generally, this would imply model deficits. In this regard, Romanowsky et al. (2019) implemented a module for fast interactive ozone chemistry into ECHAM6 improving overall stratospheric dynamics. With this improved setup, they were able to confirm the findings of Jaiser et al. (2016). In conclusion, a potential source of the inconsistency between findings from observations and modelling considering linkages between the Arctic and mid-latitudes are model deficiencies.

A different approach on explaining the model discrepancies is the question about the correct forcing that explains mid-latitude weather and climate extremes. In other words, do we do the right sensitivity experiments? Another question is, which part of the forcing has the biggest explanatory power or uncovers the biggest potential model deficit. A main focal point of this question is the so-called tug-of-war between Arctic and tropical forcing as brought up by Barnes and Screen (2015). Even inside the Arctic a distinct dependency of the impact on the specific region of SIC forcing was found (Screen, 2017).

The present study investigates the influence of sea surface temperature (SST) and SIC anomalies on the winter large-scale circulation with a focus on linkages between the Arctic and mid-latitudes in the North Atlantic and Eurasian sector. To achieve this, we perform dedicated sensitivity simulations with the atmospheric general circulation model ECHAM6. These are analyzed with a variety of methods to address the intraseasonal circulation changes in the troposphere and stratosphere and their dynamical characteristics. The sensitivity of the model to SST and SIC changes is assessed by taking differences between the variously forced model runs.

The analysis involves a focus on cyclone densities and blocking patterns, that determine much of the impacts on the weather scale from a changing climate or our sensitivity experiments, respectively. In particular blocking patterns play a major role, since they connect tropospheric changes, and thus the tropospheric pathways of polar-midlatitude linkages, to stratospheric changes, and thus the stratospheric pathway. Several studies indicate that the changes in blocking patterns and in particular their intensification lead to upward propagation of planetary waves and a consecutively disturbed stratospheric polar vortex (Colucci and Kelleher, 2015; Kim et al., 2014; Kolstad et al., 2010; Martius et al., 2009; Nishii et al., 2011). We focus on the Euro-Atlantic region, which plays a major role in particular for a more commonly displaced polar vortex (Castanheira and Barriopedro, 2010; Sun et al., 2015; Tyrlis et al., 2019).

After the description of our methods and data, we first discuss circulation changes in the troposphere by detecting and characterizing of atmospheric circulation regimes. We then further investigate the interaction between troposphere and stratosphere accompanied by a discussion of wave propagation in the critical tropopause region related to atmospheric blocking. During the analysis, the focus is on separating the influence from SST and SIC changes in relation to findings from the ERA-Interim reanalysis.

2 Data and methods

2.1 Setup of model sensitivity study

This study analyses data from four model sensitivity experiments with the atmospheric general circulation model (AGCM) ECHAM6 (Stevens et al., 2013).

We implement version 6.3 with a spectral horizontal resolution of T63 (approximately 1.875° longitude by 1.875° latitude on a Gaussian grid) and 95 vertical levels up to 0.01 hPa (approximately 80 km). The model experiments differ in their sea surface temperature (SST) and sea ice concentration (SIC) boundary forcing, while all other boundary conditions and forcing data are kept constant. The lower boundary forcing is implemented as a seasonal cycle based on monthly means and five-year averages from Merged Hadley-National Oceanic and Atmospheric Administration/Optimum Interpolation SST and SIC data set (Hurrel et al., 2008). In more detail we implement

- Low SST (LSST) from 1979 to 1983
- High SST (HSST) from 2002 to 2006
- High SIC (HICE) from 1979 to 1983
- Low SIC (LICE) from 2005 to 2009.

The forcing data of SIC has been chosen to be comparable with previous studies (Jaiser et al., 2016; Nakamura et al., 2015; Romanowsky et al., 2019). The time period of HSST differs from the time period of LICE, since we wanted to achieve more balanced changes between the state of LSST and HSST. To achieve this, we checked the indices of El Nino Southern Oscillation (ENSO, Nino-3.4 index), Pacific Decadal Oscillation (PDO) and Atlantic Multidecadal Oscillation (AMO) based on data from the Global Climate Observing System (GCOS). For the LSST average, ENSO, PDO are in a positive phase, while AMO is in a negative phase. If the LICE time period had been chosen for the HSST average, all three indices would have changed their signs. This would have resulted in too many potential sources of forcing in terms of changed large-scale circulation patterns. Therefore, the time period from 2002 to 2006 was chosen as a HSST average, where only the AMO changes to a positive phase. In this way, our results can be predominantly attributed to changes in the North Atlantic sector, our actual region of interest in this study. The general setup of model experiments with different SST and SIC conditions at the lower boundary is similar to PAMIP phase 1 experiments (Smith et al., 2019). Contrasting to them, we use forcing data related to SST and SIC change during recent decades covered by reanalysis data compared to pre-industrial, present-day and future climate forcing in PAMIP:

Combining each two mean states of SIC and SST results in four forcings for model experiments: HICE-LSST, HICE-HSST, LICE-LSST and LICE-HSST. The corresponding sensitivity experiments have been set up as time-slice experiments. The model runs 120 years with perpetual boundary forcing. The first 20 years have been discarded from the analysis to avoid any transient effects at the beginning. Five meaningful differences result from this data that allow to disentangle the effects of SIC and SST changes:

- LICE-LSST minus HICE-LSST, ice sensitivity with low SST background (ICE-LSST)
- LICE-HSST minus HICE-HSST, ice sensitivity with high SST background (ICE-HSST)
- HICE-HSST minus HICE-LSST, SST sensitivity with high ice background (SST-HICE)
- LICE-HSST minus LICE-LSST, SST sensitivity with low ice background (SST-LICE)
- LICE-HSST minus HICE-LSST, late minus early sensitivity (late-early)

Throughout the study we refer to these differences between model runs as "sensitivities".

As a reference data set, we use ERA-Interim reanalysis data (Dee et al., 2011). The data has been divided into an early period from 1979 to 2000 and a late period from 2000 to 2019. This is again done in reference to previous studies (Crasemann et al., 2017; Jaiser et al., 2012, 2013, 2016; Romanowsky et al., 2019). Both periods are separated between June and July 2000, since we are mostly interested in the winter circulation. The change between late and early period is characterized by rising SST and shrinking SIC. Therefore, the change of boundary forcing should be represented best by the difference between LICE-HSST and HICE-LSST (late-early sensitivity) from our model runs. Fig. 1 compares the averaged DJF anomalies of SIC and SST in between the late and early period in the ERA-Interim reanalysis to the corresponding differences of the forcing fields used in this study for the AGCM ECHAM6. While the patterns look generally similar amplitudes are higher for the model forcing. This is related to averaging over more years in the case of the ERA-Interim reanalysis and thus smoothing effects from more variability included.

2.2 Detection of large-scale atmospheric circulation regimes

To identify preferred atmospheric circulation regimes over the North-Atlantic-Eurasian region we applied a k-means cluster algorithm to daily mean sea level pressure (MSLP) fields of the extended winter season from December to March. ERA-Interim reanalysis data is analyzed from 1979 to 2019. The four ECHAM6 model runs HICE-LSST, HICE-HSST, LICE-LSST and LICE-HSST are corrected for shifts in their background state by removing the average MSLP field between 30° N and 90° N. Thereafter, the combined model dataset is analyzed to ensure common regimes. The circulation regimes have been determined over the region between 30°and 90° N and 90° W and 90° E. This is the main region of initiation and influence of tropospheric and stratospheric pathways linking sea ice and temperature anomalies over the Nordic seas to cold temperatures over Eurasia in winter (Hoshi et al., 2017, 2019; Kim et al., 2014; Tyrlis et al., 2019). In particular regarding the relation between blocking and stratospheric warming events, this region is of interest, since the corresponding wave flux anomalies here reaches the inside of the climatological stratospheric polar vortex (Colucci and Kelleher, 2015).

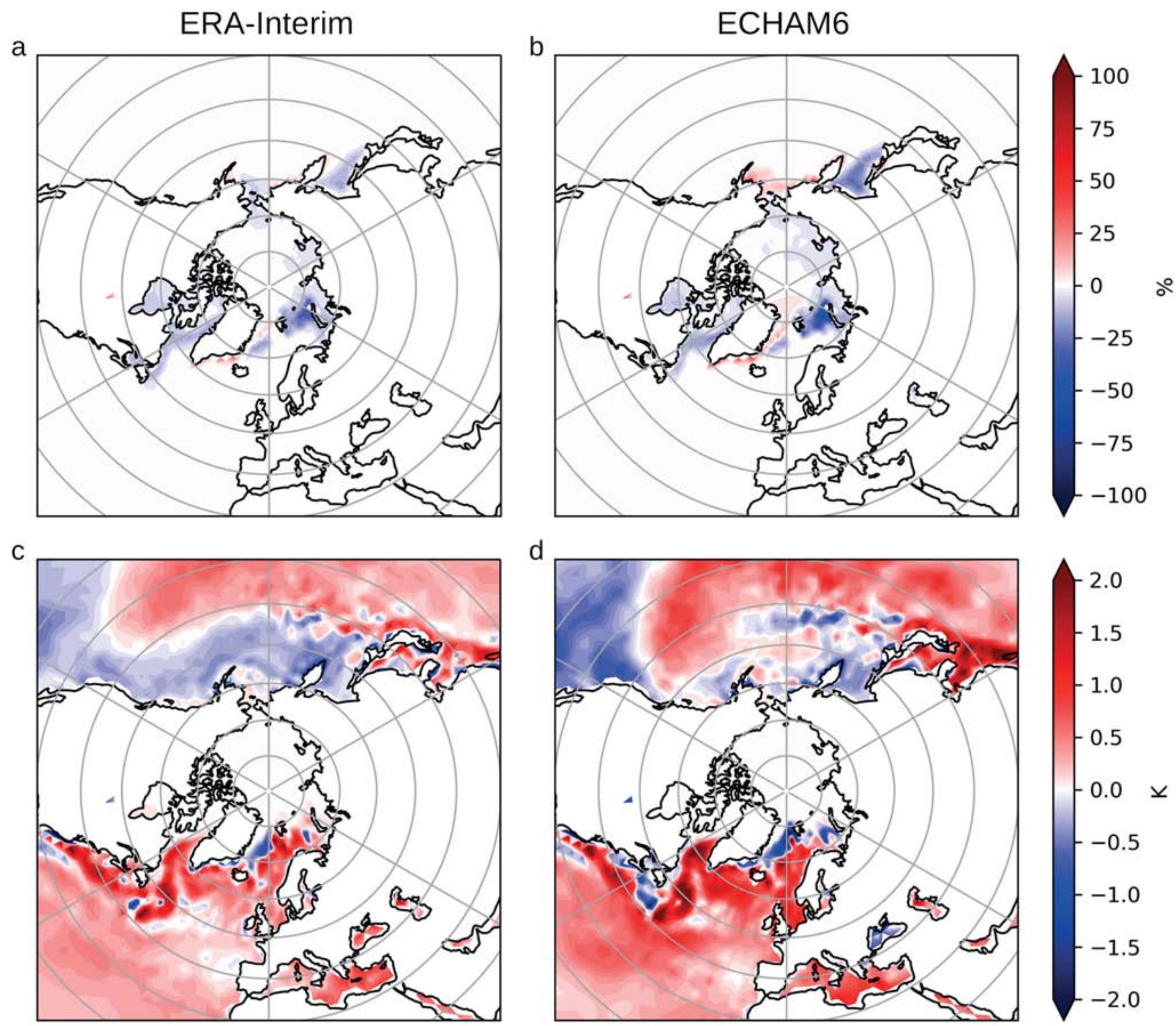

Figure 1: SIC (a, b in %) and SST (c, d row in K) anomalies averaged over December, January, February and March from ERA-Interim data. Difference between late (2000/01 to 2018/19) and early (1979/80 to 1999/2000) period as implemented in the analysis of ERA-Interim data (a, c). Difference between LICE (2005/06 to 2009/10) and HICE (1979/80 to 1983/84) (b) and HSST (2002/03 to 2006/07) and LSST (1979/80 to 1983/84) (d) as implemented in the forcing of ECHAM6 sensitivity experiments.

As in e.g., Cassou et al. (2004) and Dawson and Palmer (2015) we identify the preferred circulations regimes as non-Gaussian structures in a reduced state space and applied the same methodology as in Crasemann et al. (2017). This methodology comprises the following steps:

1. Reducing the dimensionality of the data set by an Empirical Orthogonal Function (EOF) analysis. In accordance with Crasemann et al. (2017), the subsequent steps of the analysis have been performed in the reduced state space spanned by the five leading EOF has been chosen. The five leading EOFs explain about 58 % of variance of the SLP anomaly fields for the ERA-Interim data and 55 % for the model data. The pattern correlation of each EOFs of ERA-Interim and ECHAM6 is above 0.8, showing a comparable variability of the large-scale circulation. The coordinates in this state space are provided by the corresponding, unnormalized Principal Component (PC) time series. The choice of 5 EOFs is a compromise between a large reduction of the dimension of the state space, which is necessary to efficiently perform k-means clustering in step 2, and to account for at least 50 % of the total variance in this reduced state space (in accordance with Dawson and Palmer (2015)).

2. Performing a k-means cluster analysis in the reduced state space with prescribed number of clusters k with $k = 2 \ldots 8$. This step assigns each time step of the dataset to one of the clusters, which are then interpreted as circulation regimes.

3. Testing the null hypothesis of multi-normal distribution of the probability density function by performing Monte Carlo simulations (cf. Dawson and Palmer, 2015; Straus et al., 2007) for each $k = 2 \dots 8$.

In accordance with Crasemann et al. (2017), $k = 5$ has been detected as the smallest significant partition size which is significant at the 95 % level. Extended Monte-Carlo simulations in reduced state spaces spanned by m leading EOFs ($m = 2 \dots 10$) revealed that for $m < 5$ the smallest partition size which is significant at the 95 % level is smaller than 5 but shows saturation at $k = 5$ for $m \geq 5$. Therefore, five atmospheric circulation regimes have been identified by our approach. They will be characterized based on their mean sea level pressure (MSLP) maps and cyclone and blocking densities as described in Section 2.3 and 2.4.

Differences in the relative frequency of occurrence of each circulation regime in each of the winter months have been calculated between late and early period in the ERA-Interim reanalysis and for the different model sensitivities. By applying a bootstrap test with 1000 replicates, the significance of these differences has been estimated for each regime and each month.

2.3 Detection of cyclones

The algorithm we used to identify cyclones is based on a method by Bardin and Polonsky (2005) and Akperov et al. (2007). This algorithm has been applied and compared to other methods in a number of studies dealing with changes in cyclone activity characteristics in extratropical and high latitudes (e.g., Akperov et al., 2015, 2018, 2019; Neu et al., 2013; Simmonds and Rudeva, 2014; Ulbrich et al., 2013). Cyclones were identified as low-pressure regions enclosed by closed isobars on 6-hourly maps of MSLP. The cyclone frequency was defined as the number of cyclone events per season.

To map spatial patterns of cyclone characteristics, we used a grid with circular cells of a 2.5° latitude radius. To select robust cyclone systems, cyclones with a size less than 100 km and a depth less than 1 hPa were excluded. All cyclones over regions with surface elevations higher than 1000 m were also excluded from the analysis due to large uncertainties in the MSLP fields resulting from their extrapolation to sea level. More details of this algorithm and its application for detection of the variability and changes in the cyclone activity over the Arctic have also been discussed in previous studies (e.g., Akperov et al., 2015; Zahn et al., 2018).

2.4 Detection of atmospheric blockings

Detection of atmospheric blockings was performed with the bidimensional extension of the (Tibaldi and Molteni, 1990) index developed by (Scherrer et al., 2006). It is based on reversals of the meridional gradient of the daily geopotential height at 500 hPa at every grid point between 35° N and 75° N with 2.5° step. A grid point is considered blocked when the reversal of the meridional gradient south of this grid point is observed simultaneously with the presence of a strong positive meridional gradient to the north of the same grid point for 5 or more consecutive days for at least 15° of continuous longitude.

2.5 Analysis of interaction between troposphere and stratosphere

For the analysis of large-scale circulation changes over the Arctic region and in particular the interaction between stratosphere and troposphere, we use 21-day running mean polar cap averages (zonal mean data averaged from 65° N to 88° N) of temperature. The time and height varying data is then plotted for the five abovementioned model sensitivities of the AGCM ECHAM6 and the late minus early difference of the ERA-Interim reanalysis. A nonparametric Mann-Whitney U test (Mann and Whitney, 1947) has been implemented to test for significance of the obtained differences at a 95 % confidence level together with an additional false discovery rate correction with $\alpha = 0.1$ (Benjamini and Hochberg, 1995; Wilks, 2016). Our diagnostic of vertical wave propagation is based on the vertical component of localized Eliassen Palm (EP) flux vector E_u defined in Trenberth (1986), which points in the direction of relative group velocity. The calculation of corresponding meridional heat fluxes implements covariances based on a 21-day running mean over daily data. The daily data has been treated with a 10-day low-pass filter (Blackmon and Lau, 1980) to retain only quasi-stationary planetary scale variations after the seasonal cycle had been removed. The seasonal cycle is based on the 31-day running mean data averaged over 1980 to 2018 for ERA-Interim or all years from each separate ECHAM6 model experiment, respectively. To connect blocking-related tropospheric changes to stratospheric changes, we develop a regression-based analysis between geopotential heights at 300 hPa and EP flux at 100 hPa, which is described more closely in the results section. A complementary analysis of conventional EP flux (Andrews and McIntyre, 1976) has been performed. Calculation and scaling of the cross sections is based on Jucker (2021a, b).

3 Results

3.1 Characteristics of circulation regimes

A first step of our systematic analysis is to find regimes of the atmospheric general circulation during winter (from December to March), characterize them, and compare them between model and reanalysis data. We identify the following five atmospheric circulation regimes with their MSLP anomaly patterns displayed in Fig. 2:

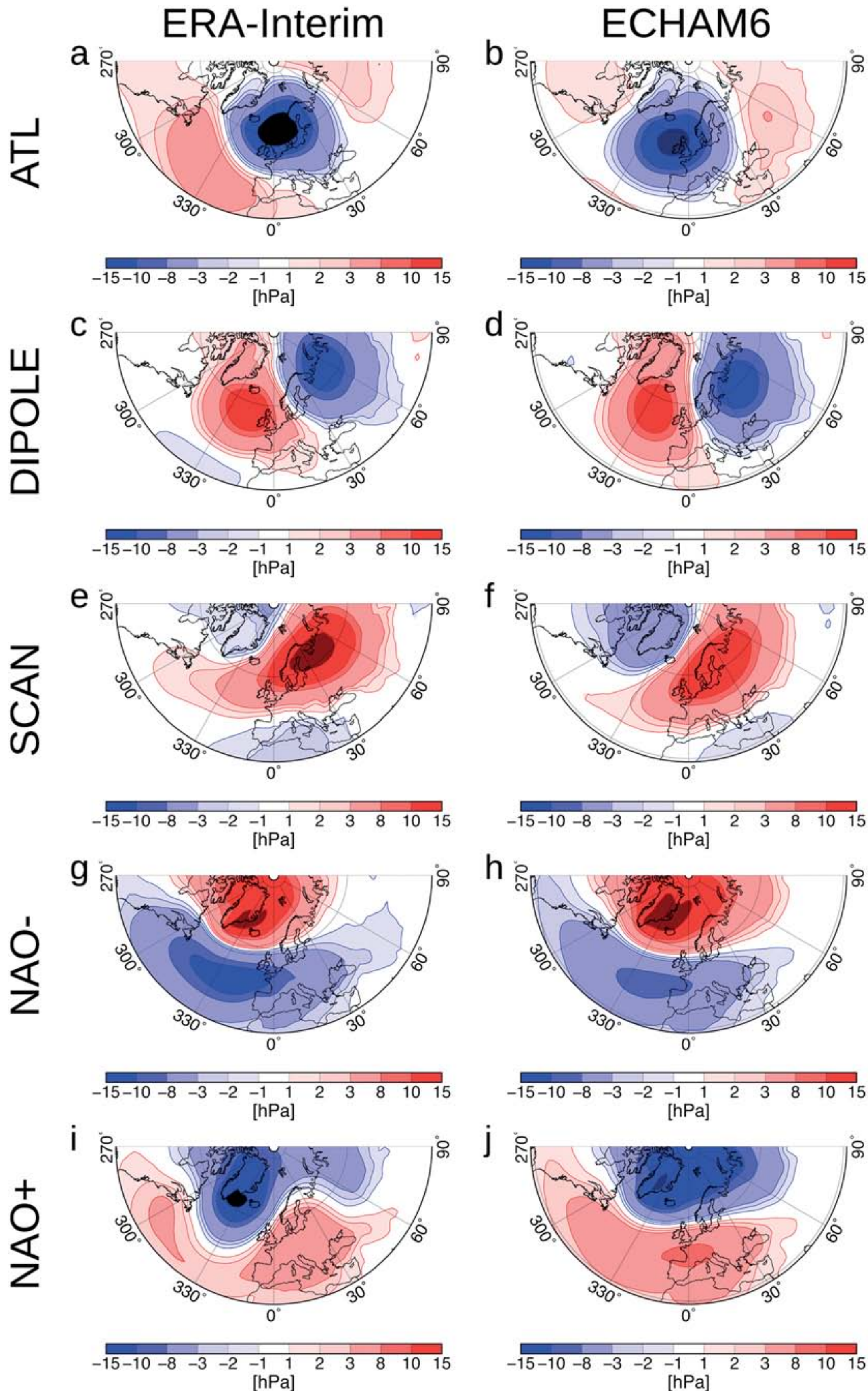

Figure 2: MSLP patterns of atmospheric circulation regimes in hPa averaged over the days assigned to the regime noted in each row derived from data of December, January, February and March in ERA-Interim (left) and ECHAM6 (right).

- Atlantic low-pressure regime (ATL, Fig. 2a, b)
- Dipole pattern regime (DIPOLE, Fig. 2c, d)
- Scandinavian/Ural blocking regime (SCAN, Fig. 2e, f)
- Negative phase of North Atlantic Oscillation (NAO−, Fig. 2g, h)
- Positive phase of North Atlantic Oscillation (NAO+, Fig. 2i, j)

In general, the patterns of all five circulation regimes show the same basic features with similar magnitudes when comparing the ERA-Interim reanalysis to the ECHAM6 model experiments. Their corresponding pattern correlations are above 0.7. This means, from an MSLP perspective, variability leads to very similar dominant large-scale circulation patterns. We performed several checks on the robustness of the determination of regimes. Instead of using the whole winter we performed the analysis for each month separately. Instead of performing the analysis for the combined set of all four model experiments, we determined regimes in each model experiment separately. Each of these checks resulted in very similar regimes. Therefore, we settled with our method of defining the atmospheric circulation regimes for the whole winter and for all model experiments together. As a result, it is ensured that they can be compared between the model runs by taking differences of their frequency of occurrence, since they are all based on the exact same definition.

In addition to the MSLP patterns we further derived the cyclone and atmospheric blocking frequencies associated with the five circulation regimes (Fig. 3 and 4). The patterns are very similar if the same regime is compared between model and reanalysis. Consistently, cyclone frequencies are reduced where higher blocking frequencies are observed and vice versa. Nevertheless, there is a general tendency of blockings to occur less frequent in ECHAM6 compared to ERA-Interim. Studies by Davini and D'Andrea (2016) and Schiemann et al. (2017) find that higher resolutions lead to more realistic blocking patterns and frequencies in models in particular in the Euro-Atlantic region. This continues to be the case in current models but considering blocking persistence the improvement of skill from higher resolution is small (Schiemann et al., 2020). In conclusion, the relatively low T63 resolution of ECHAM6 in our experiments potentially explains the bias to generally lower blocking frequencies.

Based on that data, we characterize the five atmospheric circulation regimes in the following way. The ATL pattern is generally similar to the East Atlantic / Western Russia teleconnection pattern (Eurasia-2 pattern by Barnston and Livezey, 1987) in its negative phase. Its most prominent feature is a strong negative MSLP anomaly over the North Atlantic (Fig. 2a, b). Accordingly, Figs. 3a and b show high cyclone frequencies between Greenland, south of Iceland and Scandinavia (Fig. 3a, b). At the same time, this regime is characterized by the lowest blocking activity (Fig. 4a, b). Furthermore, we note that this is the regime with the lowest pattern correlation between reanalysis and model with $r = 0.70$. The reanalysis regime (Fig. 2a) features a more meridional aligned dipole pattern over the North Atlantic. In ECHAM6 (Fig. 2b) the overall weaker positive MSLP anomalies have their centers of action on practically the same latitude as the negative MSLP anomaly. Furthermore, they are shifted to the west in comparison to the ERA-Interim reanalysis results.

The DIPOLE regime is characterized by a positive MSLP anomaly over the North Atlantic and a negative anomaly over the northern part of the Eurasian continent centered around 45° E longitude and 60° N latitude (Fig. 2c, d). Cyclones related to this circulation regime are located more north over the Barents Sea with some extensions into the continent around western Russia and a smaller maximum close to the southern tip of Greenland (Fig. 3c, d). The average blocking pattern includes a maximum frequency centered over Great Britain (Fig. 4c) or slightly shifted southwards to the Bay of Biscay in our model experiments (Fig. 4d), respectively. This is in agreement with the pressure anomaly and leads to cyclones being forced more towards the north leading to their maximum occurrence in high latitudes. Pattern correlation of MSLP between ERA-Interim (Fig. 2c) and ECHAM6 (Fig. 2d) is very high for this regime with $r = 0.91$.

The SCAN regime is characterized by a large positive MSLP anomaly centered over Scandinavia but ranging from the North Atlantic far into West Siberia (Fig. 2e, f). Correspondingly, we find a very low frequency of cyclones over Europe and Russia (Fig. 3e, f). Cyclones are bound to the region around Greenland in this circulation regime. The North Atlantic storm track extents well into the Arctic with very high cyclone frequencies west of Spitzbergen. Furthermore, cyclone frequencies are particularly low between Scandinavia and the Urals region. A corresponding maximum of high-latitude blockings is consistently found in the region of the positive pressure anomaly with its maximum over Scandinavia (Fig. 4e, f). In the ERA-Interim reanalysis, a secondary maximum is also located at the region of the Ural. Although the analysis of blockings always shows lower frequencies of occurrence in ECHAM6 compared to ERA-Interim, it is reasonably elevated in this circulation regime. The spatial correlation of the MSLP pattern between ERA-Interim (Fig. 2e) and ECHAM6 (Fig. 2f) is moderate with $r = 0.78$. This is likely due to the overall lower intensity of the high-pressure anomaly.

The NAO− regime is characterized by a positive pressure anomaly close to Iceland and negative pressure anomaly west of Europe (Fig. 2g, h). This closely resembles the well-known teleconnection pattern. For this circulation regime we detect blocking mostly over Greenland (Fig. 4g, h) that forces the North Atlantic storm tracks to the south with corresponding cyclone frequency in this region (Fig. 3g, h). At the same time, we detect higher cyclone frequencies at the Norwegian coast and over the Barents Sea. Pattern correlation of

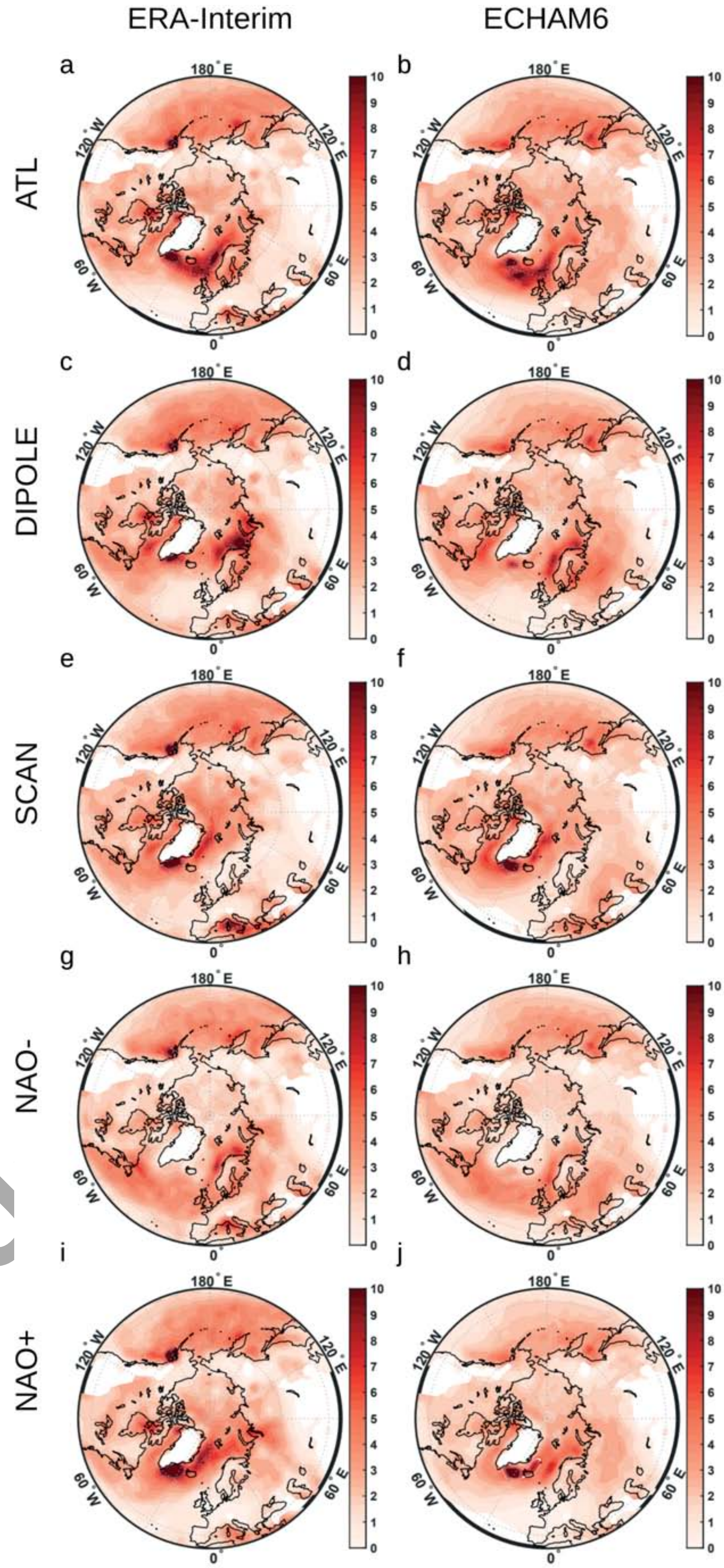

Figure 3: Cyclone frequency of atmospheric circulation regimes averaged over the days assigned to the regime noted in each row derived from data of December, January, February and March in ERA-Interim (left) and ECHAM6 (right). Frequency has been normalized to cyclones per month.

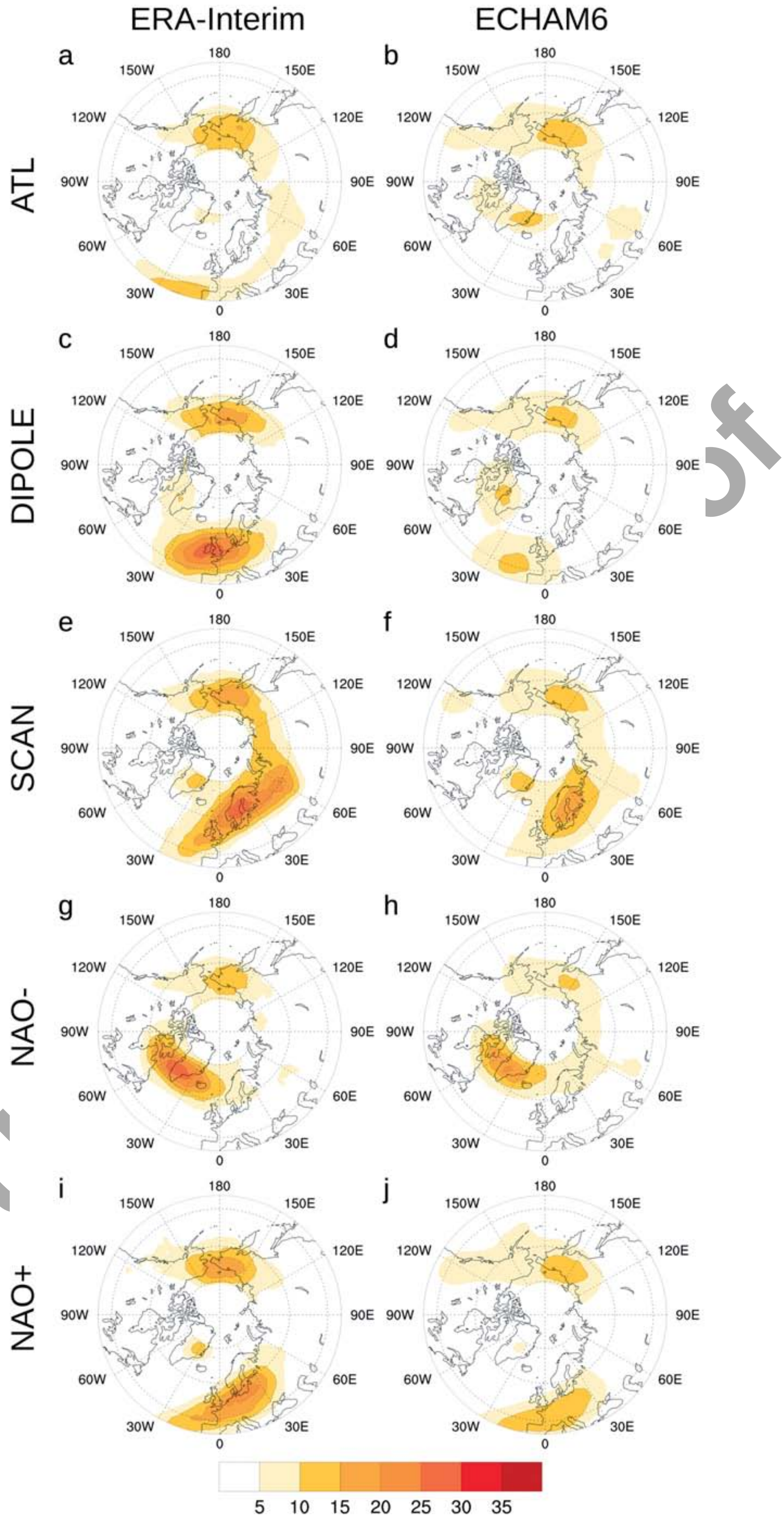

Figure 4: Blocking frequency of atmospheric circulation regimes averaged over the days assigned to the regime noted in each row derived from data of December, January, February and March in ERA-Interim (left) and ECHAM6 (right). Frequency has been normalized to blocking days per month.

MSLP between ERA-Interim (Fig. 2g) and ECHAM6 (Fig. 2h) is highest for this circulation regime with $r = 0.98$.

The NAO+ regime shows a north-south dipole of MSLP with low pressure in the north (Fig. 2i, j). Compared to the NAO− regime, the MSLP pattern is wavier and its centers of action are shifted eastward. This well-known behavior appears, if the NAO teleconnection pattern is not defined by a Principal Component Analysis (Cassou et al., 2004; Peterson et al., 2003). We find a characteristic shift of the maximum of cyclone frequency to the north extending into the Arctic North Atlantic region and reaching parts of Siberia as well (Fig. 3i, j). In particular Europe is dominated by blocking anticyclones in the mid-latitudes. Pattern correlation between the MSLP fields of ERA-Interim (Fig. 2i) and ECHAM6 (Fig. 2j) is high with $r = 0.91$, although some differences are visible in high latitude regions with a more wave-like pattern in ERA-Interim.

The circulation regimes can be grouped by their cyclonic and blocking characteristics. SCAN and NAO− show pronounced high latitude blockings. The ATL and NAO+ regimes are clearly dominated by cyclones with strong storm tracks over the North Atlantic. The DIPOLE regime is in between with relatively high cyclone frequencies in the Barents Sea region that further penetrate the continents like detected in more cyclone dominated regimes. At the same time regions more to the south are influenced by strong blocking. On the note of continental cyclones, the NAO− regime stands out as well with relatively high frequencies over eastern Europe and western Russia.

Table 1 gives the overall distribution of circulation regimes in the ERA-Interim reanalysis and the combined experiments with the ECHAM6 model. In the ERA-Interim reanalysis all regimes occur evenly distributed if accounted for the whole time series. The most frequent regime is NAO+ with 20.8 %. The NAO− regime occurs only in 18.6 % of all days during winter and is the least frequent regime. If compared to the ECHAM6 model, the ATL, DIPOLE and NAO− regimes occur at very similar frequencies around 20 %. The most frequent circulation regime in all ECHAM6 runs combined is the ATL regime with 22.6 %, which is a rather strong deviation. The least frequent regime is the NAO+ with 17.5 %, which is a clear discrepancy compared to ERA-Interim reanalysis, where NAO+ was the most frequent regime. Nevertheless, we note that NAO+ and ATL are similar regimes in terms of intense storm tracks over the Atlantic. Therefore, differences in allocation to these two regimes may not be significant in terms of shifted climatology or variability. In the following we use these identified regimes to evaluate changes in the states of the general circulation relative to our scenario runs and thus different boundary forcings.

3.2 Frequency changes of circulation regimes

Changes in the frequency of occurrence of the five different circulation regimes correspond to changes in the state of the general circulation. Quantitative differences of frequency for each sensitivity and month during winter are shown in Fig. 5. Color highlighting gives an easy view on increasing (red) and decreasing (blue) significant changes, with the intensity of the color describing the level of significance.

Table 1: Table 1: Frequency of occurrence of each regime in ERA-Interim and the combined ECHAM6 experiments in percent during the combined winter month from December to March. Differences of the sum from 100 % due to rounding errors.

Model	ATL	DIPOLE	SCAN	NAO−	NAO+
ERA-Interim	20.4	20.4	19.9	18.6	20.8
ECHAM6	22.6	20.5	20.5	19.0	17.5

Data from the ERA-Interim reanalysis shows overall fewer significant changes of frequency of the circulation regimes than the model sensitivities. Presumably, this is related to statistical effects, because the time series is shorter with only 40 years in total split into two samples that are compared. In comparison, the ECHAM6 sensitivities consist of two model runs with 100 years each. Generally, more samples lead to better statistics and robustness. Furthermore, variability is larger in the reanalysis with additional natural variability from forcing or boundary conditions that are fixed or constraint in our ECHAM6 experimental setup.

Within the ensemble of model sensitivities, the general significance of changes of regime occurrence is lower for the sensitivity on ICE compared to SST or late early. The forcing from reduced SIC has a weaker effect on the large-scale circulation than the forcing from increased SST. Reduced SIC changes the forcing of the atmosphere from higher heat fluxes from the prescribed open ocean in rather confined regions in the polar regions only. In comparison, increasing SST is a global phenomenon with a therefore stronger impact. Therefore, this result based on overall significance only is not unexpected. Still, this puts the small SIC change in a different perspective, since they are strong enough to lead to several significant circulation changes.

Analyzing the general temporal behavior of the circulation regimes, we find a notable difference between early and late winter. December and January are often consistent between the different sensitivities. It is mostly the ICE sensitivity that stands out with different signs or no significance at all. This finding is a motivation to view December and January as a combined early wintertime period. The corresponding late winter period (February and March) shows a lot more variability among the sensitivities but also between the two months.

During early winter we detect only two significant changes in regime frequencies in the ERA-Interim reanalysis data between the late and early period. The SCAN regime occurs more often in December and January, while the DIPOLE regime occurs less frequent in December only. In direct comparison this can be interpreted as a northward shift of blockings and west-

ATL

	D	J	F	M
ERA–Interim	−1.1	−0.6	1.1	−0.1
ICE–LSST	3.4	0.9	3.5	−0.8
ICE–HSST	−1.5	1.1	1.7	0.8
SST–HICE	−3.6	−1.9	−1.1	−5.6
SST–LICE	−8.5	−1.8	−2.9	−4
late–early	−5.2	−0.8	0.6	−4.7

DIPOLE

	D	J	F	M
ERA–Interim	−0.2	−7.6	0.3	6
ICE–LSST	−2.3	1.3	−2.2	−0.5
ICE–HSST	0.7	−1.5	3.2	−0.2
SST–HICE	−2.6	−0.9	−3.4	2.3
SST–LICE	0.4	−3.7	2.1	2.6
late–early	−1.9	−2.5	−0.1	2.2

SCAN

	D	J	F	M
ERA–Interim	6.2	7.8	−1.2	−11.6
ICE–LSST	−0.6	−1.5	−2.3	−0.4
ICE–HSST	1.3	0.7	2.4	−1.5
SST–HICE	3.3	2.6	−0.5	0.7
SST–LICE	5.2	4.8	4.1	−0.3
late–early	4.6	3.4	1.9	−0.7

NAO−

	D	J	F	M
ERA–Interim	−2	1.5	4.5	7
ICE–LSST	0.1	−2.9	−3.8	−2.9
ICE–HSST	−0.1	4.8	−6	2.3
SST–HICE	6.2	−1.6	1.6	−2.5
SST–LICE	6	6	−0.5	2.6
late–early	6.1	3.2	−4.3	−0.3

NAO+

	D	J	F	M
ERA–Interim	−2.9	−1	−4.8	−1.3
ICE–LSST	−0.6	2.1	4.9	4.6
ICE–HSST	−0.4	−5	−1.3	−1.5
SST–HICE	−3.2	1.8	3.3	5
SST–LICE	−3	−5.4	−2.9	−1
late–early	−3.6	−3.2	2	3.6

Figure 5: Frequency changes of circulation regimes in percent of days during the given month between periods or sensitivity runs, respectively. Names of sensitivities are indicated in Section 2.1, ERA-Interim denotes its late minus early difference. Coloring defines significance: 90 % (light), 95 % (middle), 99 % (dark).

ward shift of cyclone density over the North Atlantic. The change of the SCAN regime is reproduced by the ECHAM6 SST and late-early sensitivity. Higher SSTs result in more blockings in the Scandinavian region. In contrast, the ICE sensitivity results in no changes of SCAN frequency or even a slightly significant decrease for low SIC. Nevertheless, we note that the SST sensitivity is higher for a low SIC background based on the magnitude of frequency change. In a linear view, this might be explained by a more exposed sea surface when SIC is reduced. The decrease of frequency of the DIPOLE regime is reflected by a similar but mixed response in the ECHAM6 sensitivities. SIC reduction as well as SST increase lead to reduced DIPOLE occurrence, but with varying significance between December and January. The significant frequency change in ERA-Interim in January is only reproduced by the late-early, ICE-HSST and SST-LICE sensitivities, where for the latter ones the background state corresponds to the late state, respectively.

The ECHAM6 sensitivities show additional significant changes of regime frequencies in early winter. An increase of NAO− frequency is pronounced for the SST sensitivities. This represents a further increase of high latitude blocking patterns in conjunction with the increase in SCAN frequency. We conclude that amplified blocking patterns as detected in ERA-Interim during early winter are potentially more related to SST increase, since they primarily appear in corresponding SST sensitivities. Furthermore, their increase in frequency is at the expanse of more cyclone dominated circulation regimes like ATL and NAO+. The SIC response is more mixed without a clear general conclusion. Yet, the late-early sensitivity shows a very robust signal given that SIC decrease and SST increase operate simultaneously.

The predominant response in late winter in the ERA-Interim reanalysis is an increase of frequency of the NAO− regime. In March, we further diagnose a significant increase in the DIPOLE regime and a decrease of occurrence of the SCAN regime. This results in distribution of blockings away from Scandinavia to the west and south. This also results in higher cyclone densities in the Barents Sea region. In February there is a moderately significant shift from NAO+ to NAO− frequency. This is related to a northward shift of blockings and southward shift of storm tracks.

Model sensitivities are relatively inconsistent with these findings in late winter. The March increase in DIPOLE frequency is reproduced by SST sensitivity. We also find a consistent interplay with a decreasing ATL frequency, which results in a generally reduced cyclone density. While the ATL regime shows no significant changes in the ERA-Interim reanalysis, the NAO+ regime does show a corresponding decrease. We note here that these two circulation regimes are very similar in terms of the storm track intensity over the North Atlantic and that their overall frequency of occurrence shifts between the ERA-Interim reanalysis and the ECHAM6 model. Therefore, the shift to a reduced NAO+ regime frequency in the ERA Interim reanalysis in February and the shift to a reduced ATL regime frequency in the ECHAM6 SST sensitivities mostly in March might be related, although they are delayed.

In late winter we further detect a strong response to SIC changes. The NAO− regime occurs significantly less frequent for reduced SIC in ECHAM6, which is also dominant in the late-early response in February. The ATL regime occurs more often in terms of the SIC sensitivity in February. Therefore, we find a shift towards more North Atlantic cyclones for reduced SIC in February. This is in contradiction to the ERA-Interim result, where this shift occurs in opposite direction between the more frequent NAO− and less frequent NAO+ regime.

During late winter, a considerable dependence of the changes of regime frequency on the background conditions is observed. The NAO+ regime shows that the SIC sensitivity flips its sign if high SST background (ICE-HSST) is compared to low SST background (ICE-LSST). A similar behavior is found for the SST sensitivity if high SIC background (SST-HICE) is compared to low SIC background (SST-LICE). This implies a rather strong variability and nonlinear dependency of the results on the forcing. In comparison to ERA-Interim results, we find that these are better reproduced if the background state represents the late climate, explicitly low SIC or high SST, respectively. Regardless, much of the results considering the late winter model sensitivity are rather inconclusive. Most notably, the late-early sensitivity is more often inconsistent with the ERA-Interim findings during late winter, which was different during early winter.

In summary, SST dominates the signal in model sensitivities in terms of frequency changes of circulation regimes. This is particularly evident in early winter, when even the late-early sensitivity that involves SST and SIC change to a great extent agrees on the SST sensitivities. In early winter we detect a clear indication of higher frequency occurrence of high latitude blocking patterns. In late winter, the results are more variable and dispersed between model and reanalysis. There is a continued tendency towards less cyclone dominated regimes, with strong dependency on the type of forcing and background state. In particular changes in the regimes related to the NAO teleconnection pattern are better reflected by SST and SIC sensitivities when the background state of the other forcing corresponds to the late state, respectively. This is an indication of the importance of the interaction of SIC and SST.

Results presented here are consistent with Crasemann et al. (2017) in terms of the ERA-Interim reanalysis. In their study, they used a different model that confirmed the reanalysis results in early and late winter. The discussion of large-scale anomalies in the next sections will give some potential reasons for the differences between reanalysis data and ECHAM6 experiments.

3.3 Polar cap mean circulation characteristics

In this section, we discuss large-scale circulation changes and in particular the interaction between troposphere and stratosphere over the Arctic domain over the full seasonal cycle. The changing Arctic climate does not lead to impacts on the troposphere alone as discussed in previous sections. Previous studies showed that a changing Arctic also influences the stratospheric circulation through planetary wave propagation and polar vortex weakening (Jaiser et al., 2013, 2016; Kim et al., 2014) and these changes then feed back into the troposphere (Baldwin and Dunkerton, 2001) potentially enhancing impacts there. This is called the stratospheric pathway. Fig. 6 shows time vs. height plots of temperature averaged between 65° N and 88° N for the atmospheric column up to 10 hPa to diagnose these large-scale impacts over the Arctic. We discuss the difference between late and early period in the ERA-Interim reanalysis and the ECHAM6 model sensitivities. In ERA-Interim (Fig. 6a) we detect a general tropospheric warming and stratospheric cooling that is consistent with global warming. In January and February, an additional significant climatological warm anomaly appears in the stratosphere. This is related to more stratospheric warmings during the late period that have been related to reduced sea ice conditions in previous studies (Kretschmer et al., 2018). In March and April, we find a cold anomaly in the stratosphere potentially related to the warming in the previous months. If the vortex breaks down or is weakened in January or February, it reemerges in the following months. This reemerged vortex during late years is related to colder temperatures compared to early years when the vortex is weakened during early spring more often. Generally, the cold-warm-cold sequence of temperature anomalies encompassing a stratospheric warming is typical (see Baldwin and Dunkerton, 2001, where cold anomalies correspond to a stronger vortex and warm anomalies to a weaker vortex). Still, the question is, if other forcing like SST increase may also play a key role.

Temperature anomalies for the SIC sensitivity (Fig. 6c and d) barely show significant differences. We detect strong surface warming related to the enlarged prescribed open ocean area with more heat flux in lowermost atmosphere between September and May. Furthermore, there is some weak but significant stratospheric cooling during summer. A potential explanation is a weak uplift of the tropopause that is not significant itself. Since there is only weak variability in the stratosphere during summer, the very weak anomaly could become significant there.

SST increase has a much stronger impact on large scales as displayed in Fig. 6e and f. We detect a strong warming of the whole troposphere throughout the year. The impact of SST alone without any SIC or CO_2 changes is stronger than any tropospheric temperature changes observed in the ERA-Interim reanalysis. While we observe cold anomalies in ERA-Interim between March and December that are related to CO_2 increase, the warming extends into the stratosphere in ECHAM6 with the exception during winter. A potential explanation lies in the strength of the forcing. The difference of the forcing patterns for our low and high SST simulations (Fig. 1d) indicate stronger SST differences com-

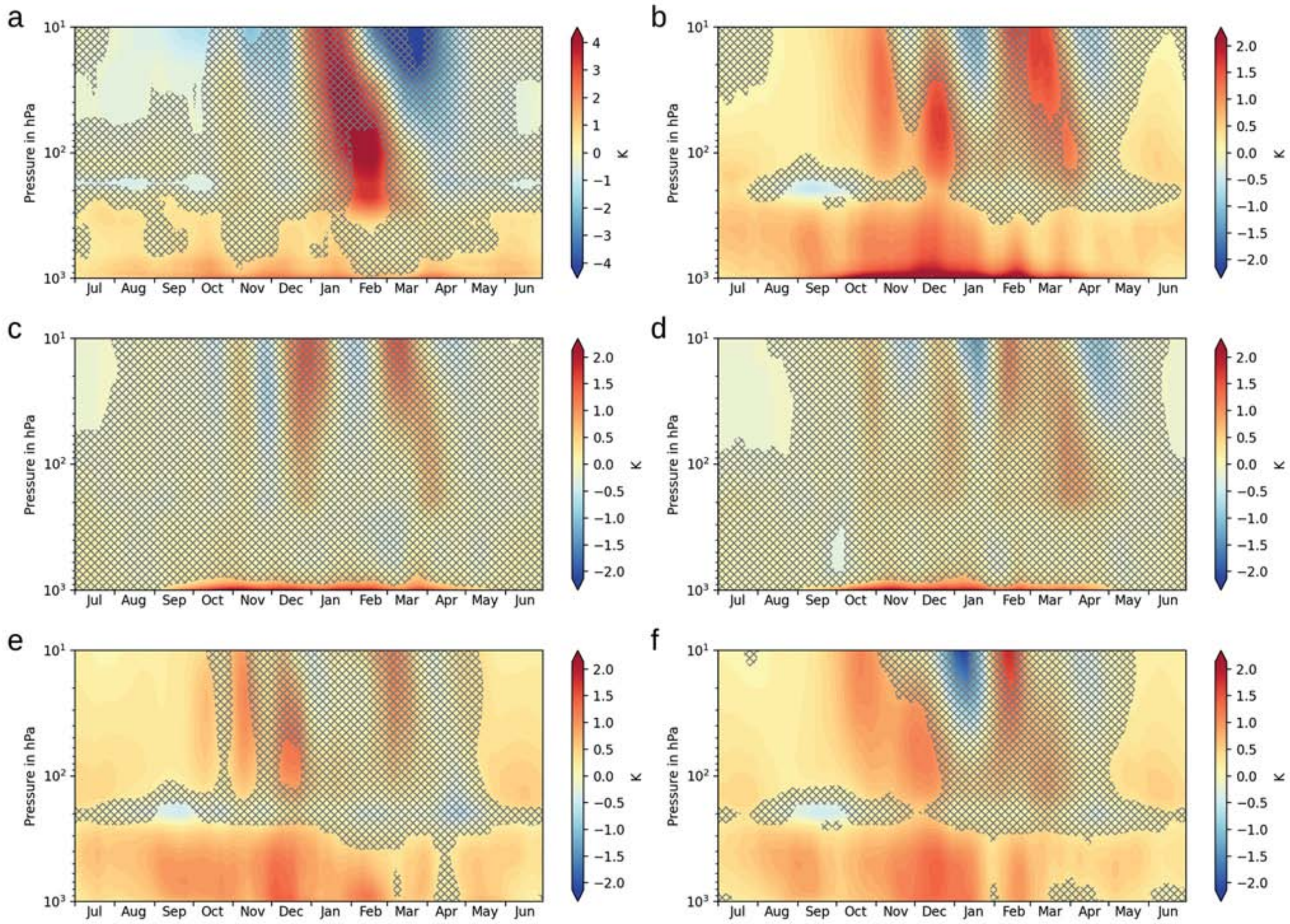

Figure 6: Temperature difference averaged over polar cap between 65° N and 88° N in K. Top row: ERA-Interim late minus early (a) and ECHAM6 late-early sensitivity implying SST increase and SIC reduction (b). Middle row, ICE sensitivity: ECHAM6 LICE minus HICE with LSST background (c) and with HSST background (d). Bottom row, SST sensitivity: ECHAM6 HSST minus LSST with HICE background (e) and LICE background (f). Differences with FDR corrected significance below 0.95 are hatched.

pared to the difference between the two time periods in ERA-Interim data (Fig. 1c). Nevertheless, the strength of the detected temperature increase throughout the atmospheric column over the Arctic is unexpectedly amplified. Additional diabatic forcing from the prescribed warmer ocean increases the heat energy content of the whole atmosphere in our experiment, where it is not set off by radiative processes from increasing CO_2 in the stratosphere or other effects. At the tropopause we find changed temperature gradients that are related to an uplift of the tropopause, consistent with a general warming. The significant warming signal in the stratosphere changes during late autumn and early winter. The amplitudes of the warm anomalies increase. This potentially indicates that higher SST and the generally warmer atmosphere led to a disturbed onset of the formation of the polar vortex. We note that this impact is more continuously detected from October to December for the low SIC background state in Fig. 6f, while for the high SIC background in Fig. 6e the significant warming signals are interrupted. The following winter is different, and we do not detect such general significant changes. Potentially, this is related to the polar stratosphere being isolated during winter with the presence of the stratospheric polar vortex.

Comparing the tropospheric impact of SST and SIC changes, we find a large difference in the extent of the warming. For changing SSTs, the whole troposphere is affected almost year-round, while for SIC changes, only the lowermost levels warm during autumn, winter, and spring. We do not find warming related to SIC changes in summer, because here the additional open sea surface is not warmer than the atmosphere. The differences in the vertical distribution of the warming are related to differences in the energy transport. Generally, the changes in SSTs are global. Thus, there is a potential of warming being advected into the Arctic from lower latitudes, which is not present when only SIC changed. Furthermore, Audette et al. (2021) discuss changes of eddy heat transport in PAMIP experiments (Smith et al., 2019), that are similarly set up with prescribed SST and SIC anomalies. They find that warming SSTs enhance the poleward eddy heat transport into the Arctic, while decreasing SIC reduces the poleward eddy heat transport into the Arctic. This effect potentially explains the differences in the middle and upper troposphere, since temperature changes in these altitude regions are more affected by advection than by local changes of boundary conditions.

In both SIC and SST sensitivities we have additional information on the impact of the background state of SST and SIC, respectively. Nevertheless, the impact of the respective background state is weak in our climatological analysis. The most prominent feature is a negative anomaly in January followed by a positive anomaly in February around 10 hPa in the SST sensitivity with low SIC background (Fig. 6f). It indicates a shift of stratospheric warmings from January to March, but without a significant impact on the lower stratosphere. Still, this increase in significant anomalies indicates that the SST impact on the winter stratosphere is more pronounced for low SIC conditions. This is further consistent with the more significant warming signal in the early winter stratosphere related to SST increase with low ice background.

Neither SST nor SIC forcing alone do explain the observed increase in stratospheric warmings during winter in the ERA-Interim reanalysis, which is why we further want to address the combined forcing. The corresponding late-early sensitivity (Fig. 6b) is generally dominated by the SST sensitivity, where we detect a general warming throughout the atmospheric column except for winter. Now, the combined SST and SIC forcing leads to a significant stratospheric warming signal in March that is comparable to ERA-Interim results but more than a month later. Arguably, this is not a very good agreement not only because of the timing difference, but also because of the differences in vertical levels that are significant. While significant differences are found in the lower stratosphere in ERA-Interim, they are found only in higher levels stratosphere in ECHAM6. Nevertheless, this result indicates that it needs forcing from higher SSTs and reduced SIC in our experiments to achieve a weak albeit significant change of the winter stratospheric circulation in terms of a warming signal.

A previous study by Romanowsky et al. (2019) analyzed the ICE-LSST sensitivity as well. They showed that by implementing a fast stratospheric ozone chemistry module, the results become more consistent with the ERA-Interim reanalysis in terms of late-winter stratospheric warming. In context of our results presented here, there are two factors that lead to a better representation of stratospheric behavior in the ECHAM6 model when compared to the ERA-Interim reanalysis: One is about the strength of the forcing anomalies and the other is about improving model dynamics and thus increasing its sensitivity. The need to address these factors is a general finding that has also been discussed in Screen et al. (2018).

The impact of the stratospheric anomalies discussed here typically is a reduced westerly circulation in the troposphere, which manifests as a negative NAM, AO or NAO (Baldwin and Dunkerton, 2001; Jaiser et al., 2016; Nakamura et al., 2015; Romanowsky et al., 2019). Here, we performed a regime analysis where negative NAO conditions are represented by one of the detected circulation regimes. In agreement with Crasemann et al. (2017) and their modelling results with a different AGCM, we detect an increase in this specific regime in February and March in the ERA-Interim reanalysis. This change of frequency is not clearly present in any of the model sensitivities. We only find an increase in NAO− frequency in March in the ICE-HSST and SST-LICE sensitivity. These are those sensitivities, where the background state represents late conditions. Although there are no significant temperature anomalies, they show some weak signs of stratospheric warmings in late winter. In terms of the late-early sensitivity, the stratospheric warming occurs later than in the reanalysis data, potentially leading to a delayed tropospheric signal. Nevertheless, an extended analysis of circulation regimes in April does not reveal any additional significant changes. This might be related to the missing significance of stratospheric signals in the lower stratosphere, indicating reduced consistent impacts on the troposphere. The inconsistent late winter results in our regime analysis might be explained by the missing impact of the stratospheric pathway or its too weak impact. Here, potential model deficits potentially play a role (Romanowsky et al., 2019).

3.4 Interaction between troposphere and stratosphere

The influence from tropospheric changes on the stratospheric circulation is carried by vertically propagation planetary waves that deposit their momentum. To diagnose this process, an analysis of conventional Eliassen-Palm flux (Andrews and McIntyre, 1976) has been performed. We show this analysis for the combined early winter period December and January, while ensuring that a monthly analysis as well as the following time period does not show any conflicting results.

Significance of the anomalies of conventional EP flux vector and its divergence is very low. Significance is shown in Fig. 7 for divergence only but is discussed here for the vector as well. In ERA-Interim, none of the anomalous vectors is significant, while divergence shows some small patchy areas of significance. The significance for the divergence is generally higher than for the vector components. The anomalous conventional EP flux vectors of ECHAM6 sensitivities are never significant if only SIC is changed. For the SST sensitivities, we find significant changes of the vectors only south of 60° N. Therefore, no significant changes of wave propagation are found in polar regions, and we cannot conclude on a relation to the stratospheric polar vortex. Correspondingly, significance of EP flux divergence is very low. It highlights some lower stratospheric areas south of 60° N and tropospheric areas south of 70° N in the SST sensitivities only. Regions in the Tropics are af-

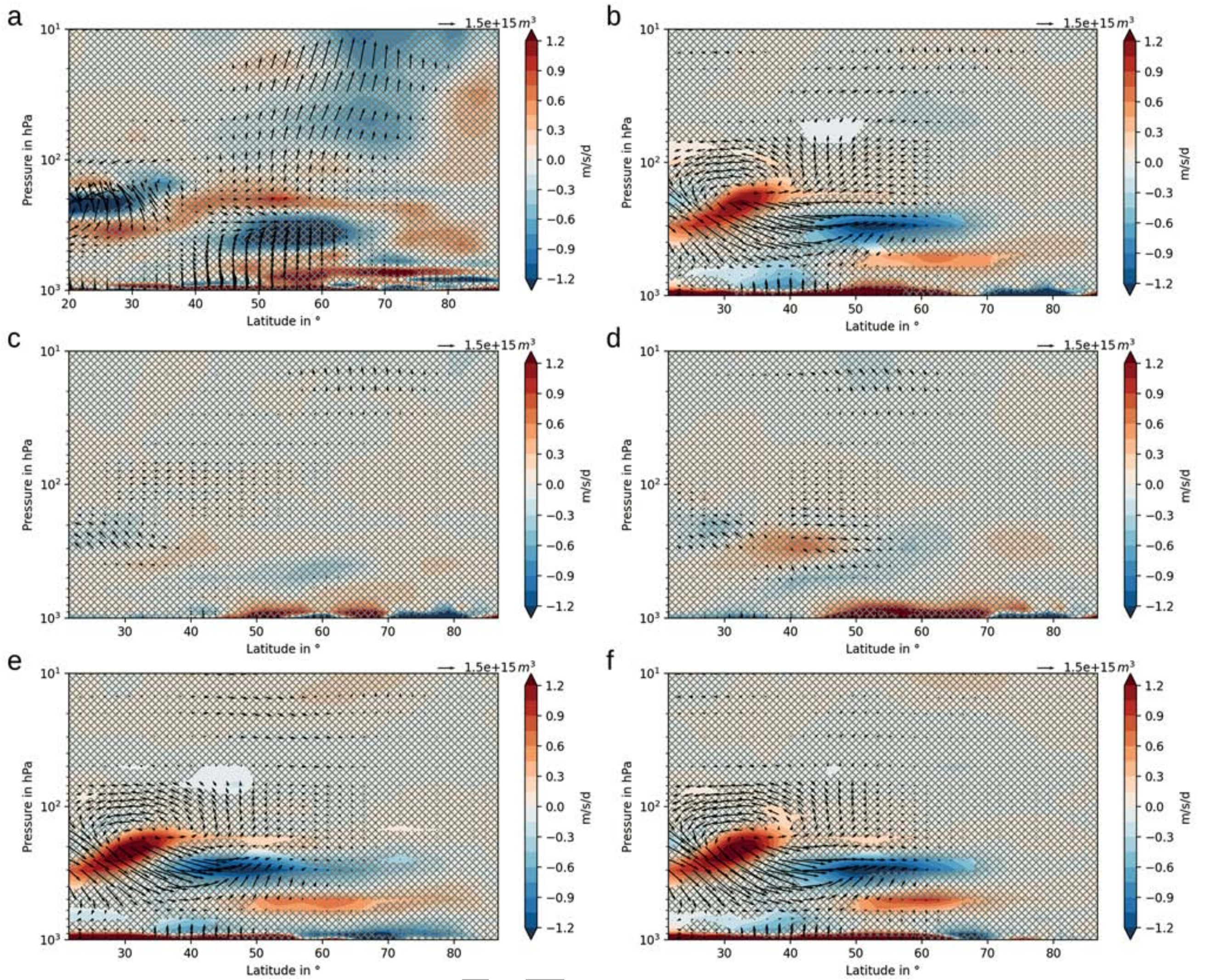

Figure 7: Conventional EP flux cross section with EP flux vector in m3 and divergence in m/s/d in early winter (DJ). Top row: ERA-Interim late minus early (a) and ECHAM6 late-early sensitivity implying SST increase and SIC reduction (b). Middle row, ICE sensitivity: ECHAM6 LICE minus HICE with LSST background (c) and with HSST background (d). Bottom row, SST sensitivity: ECHAM6 HSST minus LSST with HICE background (e) and LICE background (f). Differences of EP flux divergence with FDR corrected significance below 0.95 are hatched. Significance of the vector is not indicated, but generally lower.

fected by changing SSTs in early winter, while significant impacts on the stratospheric polar vortex region is not found.

Early winter changes of the polar stratosphere in ERA-Interim in Fig. 7a are dominated by enhanced upward conventional EP flux, while the divergence is negative. This indicates additional wave forcing from the troposphere into the stratosphere that decelerates the westerly flow. Most lower to middle tropospheric changes are diagnosed in mid to high latitudes and some very weak upward flux penetrates the critical tropopause layer between 60° N and 70° N. Further vector and divergence anomalies can be found south of 40° N. Looking at the vectors, these seem to be isolated in the subtropical higher troposphere without continuing anomalies to the stratosphere. Nevertheless, we emphasize again to be cautious with these results, since there is barely any statistical significance.

An influence on the region of the stratospheric polar vortex from changes in wave propagation is not evident from model results. Neither a change of EP flux vectors nor an anomalous divergence is diagnosed in the region north of 60° N in Figs. 7b–f. Changing SIC only does not lead to any noteworthy anomaly (Figs. 7c, d). Changing SST seems to have a relatively strong impact on the higher troposphere south of 60° N (Figs. 7b, e, f). It partially resembles some of the anomalies found in the reanalysis, with more negative divergence anomalies in mid-latitudes. In low latitudes the model shows only a positive divergence anomaly, while the counterclockwise rotation of the vector anomalies is similar to the reanalysis. In conclusion, there is some agreement between reanalysis and model in the troposphere related to SST changes, but there is no indication of an interaction between troposphere and the polar stratosphere in the model from changed lower boundary conditions.

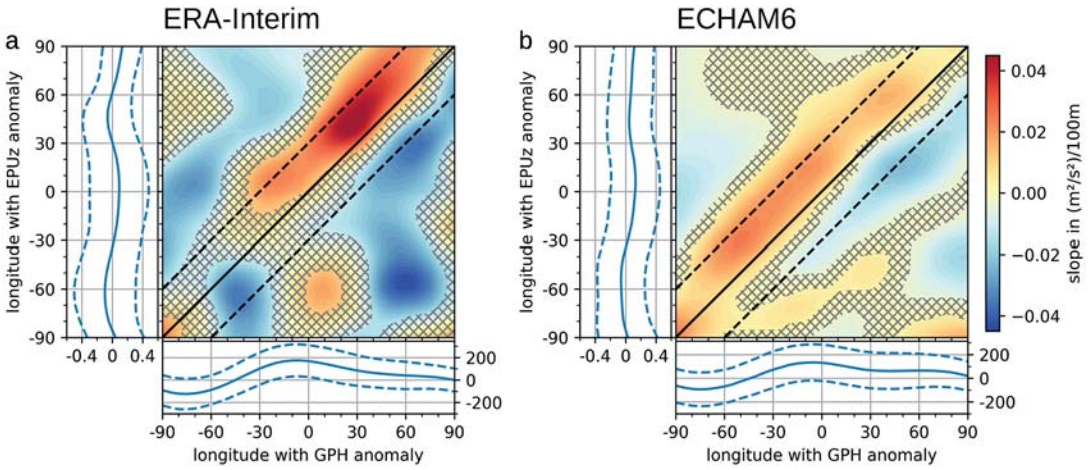

Figure 8: Regression maps between geopotential height anomalies in 300 hPa and vertical component of EP flux in 100 hPa. Daily values during December and January of both quantities are averaged for 10° longitude bins between 45° N and 88° N. Color shows regression slope between the bins of a corresponding longitude. Side panels show the climatological mean value (continuous) and added standard deviation (dashed) of geopotential height (bottom) and vertical EP flux (left), respectively. Correlation with FDR corrected significance below 0.95 is hatched.

Although not significant, the results show additional upward EP flux from the troposphere into the stratosphere and a deceleration of the zonal wind in the polar vortex region for the difference between the late and early period in the ERA-Interim reanalysis data. This is consistent with findings from the previous sections. Nevertheless, the conventional EP flux cannot resolve a regional relation between blockings and upward wave propagation. Therefore, we implement the localized EP flux (Trenberth, 1986) for a zonally resolved analysis. As a hypothesis, a local anomaly of upward EP flux could still exist in the model as well, which is masked by other opposite anomalies in other regions and thus is invisible in the zonal mean diagnostics.

3.5 Blocking induced upward wave flux

Blockings alter the large-scale tropospheric circulation and thus have the potential to change the propagation of planetary scale waves. These waves propagate vertically and potentially disturb the stratospheric polar vortex. Corresponding anomalies then propagate downwards and disturb the tropospheric circulation. This typically leads to a disturbed westerly circulation. Among others, studies by Baldwin and Dunkerton (2001), Nishii et al. (2009, 2011), Kolstad et al. (2010), Colucci and Kelleher (2015) form a basis to describe this mechanism.

Geopotential heights at 300 hPa have been found to be a good measure for Arctic anticyclones (Wernli and Papritz, 2018) generating seasonal circulation anomalies. We extend this criterion to a more hemispheric measure of anticyclonic or blocking activity. Therefore, we take daily 300 hPa geopotential heights averaged between 45° N and 88° N, remove the zonal mean and average it for 10° longitude bins.

Vertical wave flux at 100 hPa is a critical measure for wave energy that passed the tropopause region and can freely propagate into the stratosphere potentially interacting with the polar vortex. To relate it to the afore mentioned geopotential height anomalies, we take the vertical component of localized EP flux at 100 hPa and average it between 45° N to 88° N in 10° longitude bins. In comparisons to the conventional EP flux, the localized form is zonally resolved which is necessary to find potential relations to geopotential height anomalies. Jaiser et al. (2016) already showed that this localized EP flux is stronger related to the Barents Kara Sea region than in a full polar cap mean.

We now perform a regression between the data of geopotential height at 300 hPa and vertical localized EP flux at 100 hPa as described before, where the linear response of localized EP flux is derived dependent on the geopotential height anomaly. We apply this method to the time series of daily data from December and January. We further address the geographical dependency by performing the regression between all longitude bins of both variables in our region of interest between 90° W and 90° E. Thus, we identify spatial lags between both variables.

Fig. 8a shows the corresponding regression coefficients for ERA-Interim reanalysis data. The most pronounced feature is a positive regression coefficient between geopotential heights between 0° E and 60° E and vertical EP flux between 30° E and 90° E. This is the region, where the SCAN regime discussed in the regime analysis has its main center of action in terms of blockings (cf. Fig. 2e). The significant positive regression slope indicates that positive geopotential heights (blockings) are related to vertical wave propagation anomalies above the tropopause with a 10° to 30° eastward (downstream) shift. The additional vertical EP flux emerges from a region with climatological low vertical wave propagation, indicating high potential to disturb the stratospheric polar vortex. We further find negative regression coefficient that are more related to the Ural blocking around 60° E. This region of blocking is also included in the SCAN regime that occurs more often in the late time period. Negative regression coefficients indicate that vertical wave propagation further to the west around the two minima at 30° E and 60° W is reduced if blocking occurs around 60° E. In conclusion, the blocking anomalies related to a more frequent SCAN regime lead to a shift of upward wave flux from west to east. The changed position of the upward flux alters the wave-mean flow interaction and thus has the potential to impact the polar vortex differently. The sensitive region we detected here is in agreement with several previous studies (e.g. Kolstad et al., 2010; Martius et al., 2009; Nishii et al., 2011; Woollings et al., 2010). These findings show that our method is feasible to describe how increased blocking frequencies in high latitudes can initiate the stratospheric pathway.

The relation between geopotential height anomalies and vertical wave propagation is different in ECHAM6. Fig. 8b shows the corresponding regression map for all ECHAM6 experiments combined. Again, the most prominent signal is a positive regression coefficient with a 20°shift between the GPH and EP flux anomaly. This implies that the general physical mechanism is the same. Nevertheless, the maximum of the regression coefficients lies more westward and consequently does not match the region of the SCAN blocking regime or the climatological minimum of vertical wave propagation. We further note that the climatological vertical wave propagation minimum around 45° E (left side panels in Fig. 8) is not as low in the ECHAM6 model compared to the ERA-Interim reanalysis. This potentially has further implications on the general climatological behavior of the stratospheric polar vortex in ECHAM6, that is found to be too warm and thus potentially to unstable (Stevens et al. 2013). We further note that the region of negative regression coefficients in ECHAM6 related to GPH anomalies between 30° E and 60° E is similar to ERA-Interim and therefore the whole dipole structure is present. This implies that parts of the diagnosed mechanism are functional in the model, but its sensitivity is strongly reduced and appears in the wrong region in comparison to ERA-Interim, as indicated by lower regression coefficients.

Coming back to the conventional EP flux discussed more closely in Section 3.4, a lack of anomalous zonal mean wave activity in the polar stratosphere can be related to several problems. In Section 3.1 we found that ECHAM6 generally underestimates blocking frequencies. This could lead to a generally too weak forcing of wave activity. Still, the increase of blocking related regimes is well reproduced by the SST-related sensitivities (cf. Section 3.2). In addition to this, we further diagnosed a generally too weak blocking induced vertical wave fluxes in the polar regions in the model. This hints at a potential misrepresentation of interaction between waves and the mean flow in ECHAM6.

4 Conclusions

We analyzed a set of four model experiments with ECHAM6 with varying SST and SIC boundary conditions in comparison to ERA-Interim reanalysis data. The most important outcomes of the present study are:

- ECHAM6 reproduces the general patterns of the atmospheric large-scale circulation and their associated blockings and cyclone characteristics.
- Model sensitivities lack to reproduce observed changes in reanalysis data. Nevertheless, the most consistent features are found in experiments forced with concurrent SST and SIC changes.
- SIC changes alone have only a very weak impact on the large-scale circulation, likely because of a lack of vertical extent of the warming.
- SST changes have a very strong impact on temperature in the troposphere and stratosphere and lead to blocking changes in early winter similar to observations.
- Circulation changes related to SST or SIC forcing are sensitive to changes of the background state in particular during late winter.
- ECHAM6 shows discrepancies of the sensitivity of vertical wave propagation related to blocking changes in the Ural region, which is critical to reproduce the observed chain of impacts from changed boundary conditions on the stratospheric circulation.

These results show clear indications of impacts of SST and SIC changes on the large-scale circulation between the Arctic and mid-latitudes, while additional model deficits are detected. Next, we discuss these results in more detail.

Neither SIC forcing nor SST forcing alone can realistically reproduce changes in terms of linkages between polar and mid-latitudes in our model sensitivity experiments with ECHAM6 in comparison to ERA-Interim reanalysis data. SST anomalies explain much of the changes we see in early winter in terms of an increase in blocking pattern in the troposphere. Continuing into the season, only the late-early sensitivity shows significant effect on the stratospheric large-scale circulation. Thus, while not a perfect representation, the combined impact of SST and SIC changes gets closest to the results from the reanalysis. Tropospheric changes in late winter might be affected by the too weak stratospheric response. The results show that either SST increase or SIC reduction can lead to an observed increase in the frequency of the NAO− regime, but only if the background state of the other forcing is in the late state. We conclude that SIC and SST need to work together in late winter to better reproduce observations, while deficits to explain observations from the reanalysis persist throughout our whole sensitivity study.

Many models underestimate the vertical extend of observed warming of the Arctic related (Cohen et al., 2020). In nudging experiments with prescribed Arctic Amplification, Labe et al. (2020) demonstrate that sea ice forcing alone is not sufficient to reproduce the vertical extent of warming related to Arctic Amplification. In this context, our experiments show that the vertical extent of warming from SST forcing is higher, therefore fulfilling the requirements from both aforementioned studies. Still, SST forcing alone is also not sufficient, since the findings from reanalysis data are better reproduced, provided that simultaneous SIC change is prescribed.

Our experiments indicate that the strongest overall impact is related to changed SSTs. This refers in particular to a general warming of the Arctic troposphere and stratosphere, but also to changes in high-latitude blocking patterns. Higher pressure over the Arctic region and related increase in blocking frequency are consistent with the findings of Alexander et al. (2014). They diagnose a negative NAO pattern linked to a positive phase of the AMO. In terms of large-scale oceanic variability patterns, our SST sensitivity is dominated by a change from a negative AMO to a positive AMO. Consistently, we find an increase of frequency of the NAO− in early winter.

The dependence on the SIC or SST background state of the respective SST or SIC sensitivity changes during the winter season. While there is almost no dependence on the background state in early winter, we find strong variations in late winter. Generally, the impact of SST or SIC changes is better comparable to the findings in the ERA-Interim reanalysis if the background state corresponds to the late conditions, thus low SIC or high SST. Osborne et al. (2017) also performed SIC sensitivity experiments while varying the AMO background state. They only find significant impacts related to the background state in the Pacific–North American sector. Our region of interest, the Atlantic-Eurasian sector, is not influenced by the AMO state in relation to SIC sensitivity in their study. Still, the dependence on the background state strengthens our overall conclusion that the interplay of SIC and SST needs to be present to yield a realistic reproduction of observed findings.

The requirement of a combined SST and SIC forcing further indicates that the observed changes regarding linkages between the Arctic and mid-latitudes and the stratospheric pathway do not necessarily depend on changes in the Arctic alone. Our prescribed SST forcing is a global forcing not confined to the Arctic. In terms of the discussion about a “tug of war” between the Tropics and the Arctic, additional tropical forcing might strengthen impacts related to changes in the Arctic, whereas the polar stratosphere is the key component to describe changes in the North Atlantic region (Peings et al., 2019). We note that ENSO and PDO are kept in a close to constant state in our experiments, reducing the influence of these well-known large-scale drivers. We further emphasize the need for the presence of reduced SIC conditions, since the large-scale impacts are only significant with the combined forcing.

The discussion implies that forcing amplitude and origin must be correctly arranged to reproduce observed findings. As an example, Screen (2017) showed the dependence of the atmospheric response on the region of sea ice anomalies. Furthermore the amount of ice removed is important. The nonlinear response of MSLP to a stepwise decrease of SIC has been shown early on in a model study by Petoukhov and Semenov (2010). In this context, our study contrasts the efforts from the PAMIP consortium. While they implement SST and SIC forcing data corresponding to pre-industrial, present-day and future conditions, we use data from recent decades that represent currently observed changes. We further note a dependence on the model used for the sensitivity study. Our previous study Jaiser et al. (2016) implemented the AFES model instead of ECHAM6. It was able to reproduce the findings from the ERA-Interim reanalysis with only SIC forcing. Romanowsky et al. (2019) used the same model setup as in the present study and showed a weak response in ECHAM6 to SIC forcing. They realistically enhanced the response by improving the model with additional fast interactive stratospheric ozone chemistry.

We further diagnosed deficits in the response of wave propagation to changes in atmospheric blocking. Climatologically the blocking frequency in ECHAM6 is too low. Still, our analysis of circulation regimes shows a realistic change to more blockings in the Scandinavian and Ural region related to increasing SSTs. However, we find a too weak response in terms of upward propagation of planetary waves compared to the reanalysis. This is a critical process in terms of the stratospheric pathway for linkages between the Arctic and mid-latitudes. Hoshi et al. (2019) demonstrates that sea ice reduction in the Barents and Kara Sea region is a driver of the changed horizontal wave structure. This is related to blocking and leads to upward wave propagation and weak anomalies of the stratospheric polar vortex (Nishii et al., 2011). On a more general note, issues in the relation between blocking and stratospheric variability are a known issue in AGCMs (Woollings et al., 2010).

In summary, the problem is two-fold: On the one hand, we need the correct forcing. Our results indicate that both SST and SIC forcing is needed to realistically reproduce observed findings. On the other hand, models need to realistically transform the forcing into a correct response. On the latter point, Smith et al. (2020) conclude that models generally underestimate the predictable signal of the NAO by an order of magnitude. With the present study, we addressed the first problem and concluded on the requirement of more comprehensive (model) studies that either involve more detailed assessment of the relation between more complex and varied forcing the corresponding response or look deeper into processes and potential model deficits.

Acknowledgments

This study was supported by the project “Quantifying Rapid Climate Change in the Arctic: regional feedbacks and large-scale impacts (QUARCCS)" funded by the German Ministry of Research and Education (grant 03F0777A) and Ministry of Science and Higher Education of the Russian Federation (grant 14.616.21.0078 (RFMEFI61617X0078)). I. Mokhov acknowledges the support by the project funded by the Russian Science Foundation (RSF No. 19-17-00240). A. Timazhev acknowledges the support by the project funded by the Russian Science Foundation (RSF No. 19-17-00242). M.Akperov acknowledges the support by the project funded by the Russian Science Foundation (RSF No. 22-27-00780). D. Handorf is partly supported by the German Research Foundation (DFG, Deutsche Forschungsgemeinschaft) Transregional Collaborative Research Center SFB/TRR 172 "Arctic Amplification: Climate Relevant Atmospheric and Surface Processes, and Feedback Mechanisms (AC)^3" (Project-ID 268020496) and by the European Union's Horizon 2020 research and innovation framework programme under Grant agreement no. 101003590 (PolarRES). R. Jaiser is primarily supported by "Synoptic events during MOSAiC and their Forecast Reliability in the Troposphere-Stratosphere System" (SynopSys) funded by the German Federal Ministry for Education and Research (Grant/Award Number: 03F0872A) and acknowledges the support of "The linkage between POLar air-sea ice-ocean interaction, Arctic climate change and Northern hemisphere weather and climate Extremes" (POLEX) funded by the Helmholtz Association (Germany) in the priority thematic area of Climate Research (Project HRSF-0036). ERA-Interim data were obtained from the European Centre for Medium-Range Weather Forecasts (ECMWF; http://apps.ecmwf.int/datasets/data/interim_full_moda/). Data from the Global Climate Observing System (GCOS) has been obtained from National Oceanic and Atmospheric Administration Physical Sciences Laboratory (NASA PSL; https://psl.noaa.gov/gcos_wgsp/Timeseries/). The authors further want to acknowledge the Deutsches Klimarechenzentrum (DKRZ) in Hamburg for providing the general technical infrastructure for performing model runs and the analysis. The model and reanalysis data used for this paper is made available at https://cera-www.dkrz.de/WDCC/ui/cerasearch/entry?acronym=DKRZ_LTA_238_ds00002 and http://cera-www.dkrz.de/WDCC/ui/Compact.jsp?acronym=DKRZ_LTA_238_ds00003.

References

Akperov, M.G., M.Y. Bardin, E.M. Volodin, G.S. Golitsyn, I.I. Mokhov, 2007: Probability distributions for cyclones and anticyclones from the NCEP/NCAR reanalysis data and the INM RAS climate model. – Izv. Atmos. Ocean. Phys. **43**, 705–712. DOI:10.1134/S0001433807060047.

Akperov, M., I. Mokhov, A. Rinke, K. Dethloff, H. Matthes, 2015: Cyclones and their possible changes in the Arctic by the end of the twenty first century from regional climate model simulations. – Theor. Appl. Climatol. **122**, 85–96. DOI:10.1007/s00704-014-1272-2.

Akperov, M., A. Rinke, I.I. Mokhov, H. Matthes, V.A. Semenov, M. Adakudlu, J. Cassano, J.H. Christensen, M.A. Dembitskaya, K. Dethloff, X. Fettweis, J. Glisan, O. Gutjahr, G. Heinemann, T. Koenigk, N.V. Koldunov, R. Laprise, R. Mottram, O. Nikiéma, J.F. Scinocca, D. Sein, S. Sobolowski, K. Winger, W. Zhang, 2018: Cyclone activity in the Arctic from an ensemble of regional climate models (Arctic CORDEX). – J. Geophys. Res. Atmos. **123**, 2537–2554. DOI:10.1002/2017JD027703.

Akperov, M., A. Rinke, I.I. Mokhov, V.A. Semenov, M.R. Parfenova, H. Matthes, M. Adakudlu, F. Boberg, J.H. Christensen, M.A. Dembitskaya, K. Dethloff, X. Fettweis, O. Gutjahr, G. Heinemann, T. Koenigk, N.V. Koldunov, R. Laprise, R. Mottram, W. Zhang, 2019: Future projections of cyclone activity in the Arctic for the 21st century from regional climate models (Arctic-CORDEX). – Global Planetary Change **182**, 103005. DOI: 10.1016/j.gloplacha.2019.103005.

Alexander, M.A., K.H. Kilbourne, J.A. Nye, 2014: Climate variability during warm and cold phases of the Atlantic Multidecadal Oscillation (AMO) 1871–2008. – J. Marine Sys. **133**, 14–26. DOI:10.1016/j.jmarsys.2013.07.017.

Andrews, D.G., M.E. McIntyre, 1976: Planetary waves in horizontal and vertical shear: The generalized Eliassen-Palm relation and the mean zonal acceleration. – J. Atmos. Sci. **33**, 2031–2048. DOI:10.1175/1520-0469(1976)033<2031:PWIHAV>2.0.CO;2.

Audette, A., R.A. Fajber, P.J. Kushner, Y. Wu, Y. Peings, G. Magnusdottir, R. Eade, M. Sigmond, L. Sun, 2021: Opposite responses of the dry and moist eddy heat transport into the Arctic in the PAMIP experiments. – Geophys. Res. Lett. **48**, e2020GL089990. DOI:10.1029/2020GL089990.

Baldwin, M.P., T.J. Dunkerton, 2001: Stratospheric harbingers of anomalous weather regimes. – Science **294**, 581–584. DOI:10.1126/science.1063315.

Bardin, M.Y., A.B. Polonsky, 2005: North Atlantic oscillation and synoptic variability in the European- Atlantic region in winter. – Izv. Atmos. Ocean. Phys. 41, 127–136.

Barnes, E.A., J.A. Screen, 2015: The impact of Arctic warming on the midlatitude jet-stream: Can it? Has it? Will it? – Wiley Interdisciplinary Rev. Climate Change **6** 277–286. DOI: 10.1002/wcc.337.

Barnston, A.G., R.E. Livezey, 1987: Classification, seasonality and persistence of low-frequency atmospheric circulation patterns. – Mon. Wea. Rev. **115**, 1083–1126. DOI:10.1175/1520-0493(1987)115<1083:CSAPOL>2.0.CO;2.

Benjamini, Y., Y. Hochberg, 1995: Controlling the false discovery rate: a practical and powerful approach to multiple testing. – J. Roy. Statist. Soc. Ser. B, **57**, 289–300. DOI:10.1111/j.2517-6161.1995.tb02031.x.

Blackmon, M.L., N.C. Lau, 1980: Regional characteristics of the Northern Hemisphere wintertime circulation: A comparison of the simulation of a GFDL general circulation model with observations. – J. Atmos. Sci. **37**, 497–514. DOI: 10.1175/1520-0469(1980)037<0497:RCOTNH>2.0.CO;2.

Cassou, C., L. Terray, J.W. Hurrell, C. Deser, 2004: North Atlantic winter climate regimes: Spatial asymmetry, stationarity with time, and oceanic forcing. – J. Climate **17**, 1055–1068. DOI:10.1175/1520-0442(2004)017<1055:NAWCRS>2.0.CO;2.

Castanheira, J.M., D. Barriopedro, 2010: Dynamical connection between tropospheric blockings and stratospheric polar vortex. – Geophys. Res. Lett. **37**. DOI:10.1029/2010GL043819.

Cohen, J., X. Zhang, J. Francis, T. Jung, R. Kwok, J. Overland, T.J. Ballinger, U.S. Bhatt, H.W. Chen, D. Coumou, S. Feldstein, H. Gu, D. Handorf, G. Henderson, M. Ionita, M. Kretschmer, F. Laliberte, S. Lee, H.W. Linderholm, W. Maslowski, Y. Peings, K. Pfeiffer, I. Rigor, T. Semmler, J. Stroeve, P.C. Taylor, S. Vavrus, T. Vihma, S. Wang, M. Wendisch, Y. Wu, J. Yoon, 2020: Divergent consensuses on Arctic amplification influence on midlatitude severe winter weather. – Nature Climate Change **10**, 20–29. DOI:10.1038/s41558-019-0662-y.

Colucci, S.J., M.E. Kelleher, 2015: Diagnostic comparison of tropospheric blocking events with and without sudden stratospheric warming. – J. Atmos. Sci. **72**, 2227–2240. DOI: 10.1175/JAS-D-14-0160.1.

Crasemann, B., D. Handorf, R. Jaiser, K. Dethloff, T. Nakamura, J. Ukita, K. Yamazaki, 2017: Can preferred atmospheric circulation patterns over the North-Atlantic-Eurasian region be associated with arctic sea ice loss? – Polar Sci. **14**, 9–20. DOI:10.1016/j.polar.2017.09.002.

Davini, P., F. D'Andrea, 2016: Northern Hemisphere atmospheric blocking representation in global climate models: Twenty years of improvements? – J. Climate **29**, 8823–8840. DOI:10.1175/JCLI-D-16-0242.1.

Dawson, A., T.N. Palmer, 2015: Simulating weather regimes: Impact of model resolution and stochastic parameterization. – Climate Dynam. **44**, 2177–2193. DOI:10.1007/s00382-014-2238-x.

Day, J.J., M.M. Holland, K.I. Hodges, 2018: Seasonal differences in the response of Arctic cyclones to climate change in CESM1. – Climate Dynam. **50**, 3885–3903. DOI:10.1007/s00382-017-3767-x.

Dee, D.P., S.M. Uppala, A.J. Simmons, P. Berrisford, P. Poli, S. Kobayashi, U. Andrae, M.A. Balmaseda, G. Balsamo, P. Bauer, P. Bechtold, A.C.M. Beljaars, L. van de Berg, J. Bidlot, N. Bormann, C. Delsol, R. Dragani, M. Fuentes, A.J. Geer, L. Haimberger, S.B. Healy, H. Hersbach, E.V. Hólm, L. Isaksen, P. Kållberg, M. Köhler, M. Matricardi, A.P. McNally, B.M. Monge-Sanz, J.-J. Morcrette, B.-K. Park, C. Peubey, P. de Rosnay, C. Tavolato, J. -N. Thépaut, F. Vitart, 2011: The ERA-Interim reanalysis: Configuration and performance of the data assimilation system. – Quart. J.Roy. Meteor. Soc. **137**, 553–597. DOI:10.1002/qj.828.

Francis, J.A., S.J. Vavrus, 2012: Evidence linking Arctic amplification to extreme weather in mid-latitudes. – Geophys. Res. Lett. **39**, L06801. DOI:10.1029/2012GL051000.

Handorf, D., R. Jaiser, K. Dethloff, A. Rinke, J. Cohen, 2015: Impacts of Arctic sea ice and continental snow cover changes on atmospheric winter teleconnections. – Geophys. Res. Lett. **42**, 2367–2377. DOI:10.1002/2015GL063203.

He, Y., J. Huang, M. Ji, 2014: Impact of land–sea thermal contrast on interdecadal variation in circulation and blocking. – Climate Dynam. 43, 3267–3279. DOI:10.1007/s00382-014-2103-y.

Hoshi, K., J. Ukita, M. Honda, K. Iwamoto, T. Nakamura, K. Yamazaki, K. Dethloff, R. Jaiser, D. Handorf, 2017: Poleward eddy heat flux anomalies associated with recent Arctic sea ice loss. – Geophys. Res. Lett. 44, 446–454. DOI: 10.1002/2016GL071893.

Hoshi, K., J. Ukita, M. Honda, T. Nakamura, K. Yamazaki, Y. Miyoshi, R. Jaiser, 2019: Weak stratospheric polar vortex events modulated by the Arctic sea-ice loss. – J. Geophys. Res. Atmos. **124**, 858–869. DOI:10.1029/2018JD029222.

Jaiser, R., K. Dethloff, D. Handorf, A. Rinke, J. Cohen, 2012: Impact of sea ice cover changes on the Northern Hemisphere atmospheric winter circulation. – Tellus A **64**, 11595. DOI:10.3402/tellusa.v64i0.11595.

Jaiser, R., K. Dethloff, D. Handorf, 2013: Stratospheric response to Arctic sea ice retreat and associated planetary wave propagation changes. – Tellus A **65**, 19375. DOI:10.3402/tellusa.v65i0.19375.

Jaiser, R., T. Nakamura, D. Handorf, K. Dethloff, J. Ukita, K. Yamazaki, 2016: Atmospheric winter response to Arctic sea ice changes in reanalysis data and model simulations. – J. Geophys. Res. Atmos. **121**, 7564–7577. DOI: 10.1002/2015JD024679.

Jucker, M., 2021a: Scaling of Eliassen-Palm flux vectors. – Atmos. Sci. Lett. **22**, e1020. DOI:extdoi10.1002/asl.1020.

Jucker, M., 2021b: mjucker/aostools: v2.3.2 (Version v2.3.2). – Zenodo. DOI:10.5281/zenodo.4588067.

Jung, T., N.D. Gordon, P. Bauer, D.H. Bromwich, M. Chevallier, J.J. Day, J. Dawson, F. Doblas-Reyes, C. Fairall, H.F. Goessling, M. Holland, J. Inoue, T. Iversen, S. Klebe, P. Lemke, M. Losch, A. Makshtas, B. Mills, P. Nurmi, D. Perovich, P. Reid, I.A. Renfrew, G. Smith, G. Svensson, M. Tolstykh, Q. Yang, 2016: Advancing polar prediction capabilities on daily to seasonal time scales. – Bull. Amer. Meteor. Soc. **97**, 1631–1647. DOI:10.1175/BAMS-D-14-00246.1.

Kim, B.M., S.W. Son, S.K. Min, J.H. Jeong, S.J. Kim, X. Zhang, T. Shim, J.H. Yoon, 2014: Weakening of the stratospheric polar vortex by Arctic sea-ice loss. – Nature Comm. **5**, 1–8. DOI:10.1038/ncomms5646.

Kolstad, E.W., T. Breiteig, A.A. Scaife, 2010: The association between stratospheric weak polar vortex events and cold air outbreaks in the Northern Hemisphere. – Quart. J. Roy. Meteor. Soc. **136**, 886–893. DOI:10.1002/qj.620.

Kretschmer, M., D. Coumou, L. Agel, M. Barlow, E. Tziperman, J. Cohen, 2018: More-persistent weak stratospheric polar vortex states linked to cold extremes. – Bull. Amer. Meteor. Soc. **99**, 49–60. DOI:10.1175/BAMS-D-16-0259.1.

Labe, Z., Y. Peings, G. Magnusdottir, 2020: Warm Arctic, Cold Siberia Pattern: Role of Full Arctic Amplification Versus Sea Ice Loss Alone. – Geophys. Res. Lett. **47**, e2020GL088583. DOI:10.1029/2020GL088583.

Lupo, A.R., R.J. Oglesby, I.I. Mokhov, 1997: Climatological features of blocking anticyclones: A study of Northern Hemisphere CCM1 model blocking events in present-day and double CO2 concentration atmospheres. – Climate Dynam. **13**, 181–195. DOI:10.1007/s003820050159.

Mann, H.B., D.R. Whitney, 1947: On a test of whether one of two random variables is stochastically larger than the other. – Ann. Math. Stat. **50–60**. DOI:10.1214/aoms/1177730491.

Martius, O., L.M. Polvani, H.C. Davies, 2009: Blocking precursors to stratospheric sudden warming events. – Geophys. Res. Lett. **36**. DOI:10.1029/2009GL038776.

Mokhov, I.I., V.K. Petukhov, 1997: Blockings and tendencies of their change. – Dokl. Earth Sci. A, **357**, 1485–1488.

Mokhov, I.I., V.A. Semenov, 2016: Weather and climate anomalies in Russian regions related to global climate change. – Russ. Meteor. Hydrol. **41**, 84–92. DOI:10.3103/S1068373916020023.

Nakamura, T., K. Yamazaki, K. Iwamoto, M. Honda, Y. Miyoshi, Y. Ogawa, J. Ukita, 2015: A negative phase shift of the winter AO/NAO due to the recent Arctic sea-ice reduction in late autumn. – J. Geophys. Res. Atmos. **120**, 3209–3227. DOI:10.1002/2014JD022848.

Neu, U., M.G. Akperov, N. Bellenbaum, R. Benestad, R. Blender, R. Caballero, A. Cocozza, H.F. Dacre, Y. Feng, K. Fraedrich, J. Grieger, S. Gulev, J. Hanley, T. Hewson, M. Inatsu, K. Keay, S.F. Kew, I. Kindem, G.C. Leckebusch, M.L.R. Liberato, P. Lionello, I.I. Mokhov, J.G. Pinto, C.C. Raible, M. Reale, I. Rudeva, M. Schuster, I. Simmonds, M. Sinclair, M. Sprenger, N.D. Tilinina, I.F. Trigo, S. Ulbrich, U. Ulbrich, X.L. Wang, H. Wernli, 2013: IMILAST: A community effort to intercompare extratropical cyclone detection and tracking algorithms. – Bull. Amer. Meteor. Soc. **94**, 529–547. DOI:10.1175/BAMS-D-11-00154.1.

Nishii, K., H. Nakamura, T. Miyasaka, 2009: Modulations in the planetary wave field induced by upward-propagating Rossby wave packets prior to stratospheric sudden warming events: A case-study. – Quart. J. Roy. Meteor. Soc. **135**, 39–52. DOI:10.1002/qj.359.

Nishii, K., H. Nakamura, Y.J. Orsolini, 2011: Geographical dependence observed in blocking high influence on the stratospheric variability through enhancement and suppression of upward planetary-wave propagation. – J. Climate **24**, 6408–6423. DOI:10.1175/JCLI-D-10-05021.1.

Osborne, J.M., J.A. Screen, M. Collins, 2017: Ocean-atmosphere state dependence of the atmospheric response to Arctic sea ice loss. – J. Climate **30**, 1537–1552. DOI:10.1175/JCLI-D-16-0531.1.

Overland, J.E., T.J. Ballinger, J. Cohen, J.A. Francis, E. Hanna, R. Jaiser, B.M. Kim, S.J. Kim, J. Ukita, T. Vihma, M. Wang, X. Zhang, 2021: How do intermittency and simultaneous processes obfuscate the Arctic influence on midlatitude winter extreme weather events? – Env. Res. Lett. **16**, 043002. DOI:10.1088/1748-9326/abdb5d.

Peings, Y., J. Cattiaux, G. Magnusdottir, 2019: The Polar Stratosphere as an Arbiter of the Projected Tropical Versus Polar Tug of War. – Geophys. Res. Lett. **46**, 9261–9270. DOI:10.1029/2019GL082463.

Peterson, K.A., J. Lu, R.J. Greatbatch, 2003: Evidence of nonlinear dynamics in the eastward shift of the NAO. – Geophs. Res. Lett. **30**, 1030. DOI:10.1029/2002GL015585.

Petoukhov, V., V.A. Semenov, 2010: A link between reduced Barents-Kara sea ice and cold winter extremes over northern continents. – J. Geophys. Res. **115**, D21111. DOI:10.1029/2009JD013568.

Romanowsky, E., D. Handorf, R. Jaiser, I. Wohltmann, W. Dorn, J. Ukita, J. Cohen, M. Rex, 2019: The role of stratospheric ozone for Arctic-midlatitude linkages. – Sci. Rep. **9**, 7962. DOI:10.1038/s41598-019-43823-1.

Screen, J.A., 2017: Simulated atmospheric response to regional and pan-Arctic sea ice loss. – J. Climate **30**, 3945–3962. DOI:10.1175/JCLI-D-16-0197.1.

Screen, J.A., C. Deser, D.M. Smith, X. Zhang, R. Blackport, P.J. Kushner, T. Oudar, K.E. McCusker, L. Sun, 2018: Consistency and discrepancy in the atmospheric response to Arctic sea-ice loss across climate models. – Nature Geosci. **11**, 155-163. DOI:10.1038/s41561-018-0059-y.

Scherrer, S.C., M. Croci-Maspoli, C. Schwierz, C. Appenzeller, 2006: Two-dimensional indices of atmospheric blocking and their statistical relationship with winter climate patterns in the Euro-Atlantic region. – Int. J. Climatol. **26**, 233–249. DOI:10.1002/joc.1250.

Schiemann, R., M.E. Demory, L.C. Shaffrey, J. Strachan, P.L. Vidale, M.S. Mizielinski, M.J. Roberts, M. Matsueda, M.F. Wehner, T. Jung, 2017: The resolution sensitivity of Northern Hemisphere blocking in four 25-km atmospheric global circulation models. – J. Climate **30**, 337–358. DOI:10.1175/JCLI-D-16-0100.1.

Schiemann, R., P. Athanasiadis, D. Barriopedro, F. Doblas-Reyes, K. Lohmann, M.J. Roberts, D.V. Sein, C.D. Roberts, L. Terray, P.L. Vidale, 2020: Northern Hemisphere blocking simulation in current climate models: evaluating progress from the Climate Model Intercomparison Project Phase 5 to 6 and sensitivity to resolution. – Wea. Climate Dynam. **1**, 277–292. DOI:10.5194/wcd-1-277-2020.

Simmonds, I., I. Rudeva, 2014: A comparison of tracking methods for extreme cyclones in the Arctic basin. – Tellus A **66**, 25252. DOI:10.3402/tellusa.v66.25252.

Smith, D.M., J.A. Screen, C. Deser, J. Cohen, J.C. Fyfe, J. García-Serrano, T. Jung, V. Kattsov, D. Matei, R. Msadek, Y. Peings, M. Sigmond, J. Ukita, J.H. Yoon, X. Zhang, 2019: The Polar Amplification Model Intercomparison Project (PAMIP) contribution to CMIP6: Investigating the causes and consequences of polar amplification. – Geosci. Model Develop. **12**, 1139–1164. DOI:10.5194/gmd-12-1139-2019.

Smith, D.M., A.A. Scaife, R. Eade, P. Athanasiadis, A. Bellucci, I. Bethke, R. Bilbao, L.F. Borchert, L.-P. Caron, F. Counillon, G. Danabasoglu, T. Delworth, F.J. Doblas-Reyes, N.J. Dunstone, V. Estella-Perez, S. Flavoni, L. Hermanson, N. Keenlyside, V. Kharin, M. Kimoto, W.J. Merryfield, J. Mignot, T. Mochizuki, K. Modali, P.-A. Monerie, W.A. Müller, D. Nicolí, P. Ortega, K. Pankatz, H. Pohlmann, J. Robson, P. Ruggieri, R. Sospedra-Alfonso, D. Swingedouw, Y. Wang, S. Wild, S. Yeager, X. Yang, L. Zhang, 2020: North Atlantic climate far more predictable than models imply. – Nature **583**, 796–800. DOI:10.1038/s41586-020-2525-0.

Stevens, B., M. Giorgetta, M. Esch, T. Mauritsen, T. Crueger, S. Rast, M. Salzmann, H. Schmidt, J. Bader, K. Block, R. Brokopf, I. Fast, S. Kinne, L. Kornblueh, U. Lohmann, R. Pincus, T. Reichler, E. Roeckner, 2013: Atmospheric component of the MPI-M Earth system model: ECHAM6. – J. Adv. Model. Earth Sys. **5**, 146–172. DOI:10.1002/jame.20015.

Straus, D.M., S. Corti, F. Molteni, 2007: Circulation regimes: Chaotic variability versus SST-forced predictability. – J. Climate **20**, 2251–2272. DOI:10.1175/JCLI4070.1.

Sun, L., C. Deser, R.A. Tomas, 2015: Mechanisms of stratospheric and tropospheric circulation response to projected Arctic sea ice loss. – J. Climate **28**, 7824–7845. DOI:10.1175/JCLI-D-15-0169.1.

Tibaldi, S., F. Molteni, 1990: On the operational predictability of blocking. – Tellus A, **42**, 343–365. DOI:10.3402/tellusa.v42i3.11882.

Trenberth, K. E, 1986: An assessment of the impact of transient eddies on the zonal flow during a blocking episode using localized Eliassen-Palm flux diagnostics. – J. Atmos. Sci. **43**, 2070–2087. DOI:10.1175/1520-0469(1986)043<2070:AAOTIO>2.0.CO;2.

Tyrlis, E., E. Manzini, J. Bader, J. Ukita, H. Nakamura, D. Matei, 2019: Ural blocking driving extreme Arctic sea ice loss, cold Eurasia, and stratospheric vortex weakening in autumn and early winter 2016–2017. – J. Geophys. Res. Atmos. **124**, 11313–11329. DOI:10.1029/2019JD031085.

Ulbrich, U., G.C. Leckebusch, J. Grieger, M. Schuster, M. Akperov, M.Y. Bardin, Y. Feng, S. Gulev, M. Inatsu, K. Keay, S.F. Kew, M.L. R. Liberato, P. Lionello, I.I. Mokhov, U. Neu, J.G. Pinto, C.C. Raible, M. Reale, I. Rudeva, I. Simmonds, N.D. Tilinina, I.F. Trigo, S. Ulbrich, X.L. Wang, H. Wernli, 2013: Are greenhouse gas signals of Northern Hemisphere winter extra-tropical cyclone activity dependent on the identification and tracking algorithm?. – Meteorol. Z. **22**, 61–68. DOI:10.1127/0941-2948/2013/0420.

Wendisch, M. Brückner, J.P. Burrows, S. Crewell, K. Dethloff, K. Ebell, C. Lüpkes, A. Macke, J. Notholt, J. Quaas, A. Rinke, I. Tegen, 2017: Understanding causes and effects of rapid warming in the Arctic. – Eos, **98**, published online. DOI:10.1029/2017EO064803.

Wernli, H., L. Papritz, 2018: Role of polar anticyclones and mid-latitude cyclones for Arctic summertime sea-ice melting. – Nature Geosci. **11**, 108–113. DOI:10.1038/s41561-017-0041-0.

Wilks, D., 2016: "The stippling shows statistically significant grid points": How research results are routinely overstated and overinterpreted, and what to do about it. – Bull. Amer. Meteor. Soc. **97**, 2263–2273. DOI:10.1175/BAMS-D-15-00267.1.

Woollings, T., A. Charlton-Perez, S. Ineson, A.G. Marshall, G. Masato, 2010: Associations between stratospheric variability and tropospheric blocking. – J. Geophys. Res. Atmos. **115**, published online. DOI:10.1029/2009JD012742.

Zahn, M., M. Akperov, A. Rinke, F. Feser, I.I. Mokhov, 2018: Trends of cyclone characteristics in the Arctic and their patterns from different reanalysis data. – J. Geophys. Res. Atmos. **123**, 2737–2751. DOI:10.1002/2017JD027439.